공학박사학위논문

Terrain Referenced Navigation with State Augmentation Using Adaptive Two Stage Point Mass Filter

적응 2 단계 PMF 를 이용한 지형 참조 항법의 상태 변수 확장

2019 년 2 월

서울대학교 대학원

기계항공공학부

박 용 곤 종

Abstract

Terrain Referenced Navigation with State Augmentation Using Adaptive Two Stage Point Mass Filter

Yong-gonjong Park
Department of Mechanical and Aerospace Engineering
The Graduate School
Seoul National University

In this dissertation, a novel approach by the adaptive two stage point mass filter (ATSPMF) is proposed for improving computation efficiency and estimation performance in point mass filter (PMF) based terrain referenced navigation (TRN). The inertial navigation system (INS) is provides the position, velocity and attitude of the vehicle based on dead reckoning with an inertial measurement unit (IMU) alone. INS has advantages for small short term error, high update frequency and robustness of external disturbance, but it has a fatal disadvantage that it diverges

over time. To overcome this problem, INS should be aided by another sensor that provides absolute position or other information that can be used to estimate position such as global positioning system (GPS). INS aided GPS is the most widely used for integrated navigation system because it can be configured easily and estimates position, velocity, attitude and bias error of the IMU by only GPS position information as a measurement of the Kalman filter. In recently, however, GPS can be disturbed by jamming or spoofing and it may lost reliability or become unusable.

The TRN is a navigation system suitable for alternative navigation system for INS aided GPS. It uses the difference between measured terrain elevation which received by radar altimeter (RA) and barometric altimeter (BA) and terrain elevation information provided by digital elevation map (DEM) as a measurement of the TRN. Also, the TRN uses the nonlinear filter such as the PMF by using the measurement mentioned above because the nonlinearity of the measurement is severe. For improving PMF based TRN, I have proposed the novel approaches by grid support adaptation and two stage filtering.

First, I have proposed adaptive grid support algorithm for improving estimation performance and computation efficiency in PMF based TRN. In general PMF based TRN, the size of the grid support is maintained constantly. But that simple way has some disadvantages for computation burden and estimation performance. So, I have proposed new grid support adaptation method which can consider the roughness of the terrain elevation and accuracy of the measurement by using mutual information (MI) as an adaptation index. The adaptation index determines whether to increase the size of the grid support or decrease.

Second, the two stage PMF (TSPMF) is proposed for state augmentation with computation efficiency. For improving estimation performance of PMF based TRN itself, it is advantageous to set more state variables. But, the more state variables, the more computational burden exponentially. The TSPMF can provide great efficiency with state augmentation by two stages. In first stage, the nonlinear state variables are estimated by general PMF. Next, in second stage, the linear state variables are estimated by a single Kalman filter. At this time, some information that can be obtained by PMF in first stage is used in second stage for considering the correlation nonlinear and linear state variables.

In simulation results, the estimation performance and computational efficiency is improved by grid support adaptation in two dimensional state variables PMF and TRN. Also, when the state variables are augmented by three dimensions, the computation efficiency is improved by TSPMF as the estimation performance is maintained.

Keywords: Terrain referenced navigation, Point mass filter, Grid adaptation, Measurement quality, two stage filtering, state augmentation

Student number: 2014-30363

Contents

List of Figures

List of Tables

Chapter 1

Introduction

1.1 Motivation and Background

In this dissertation, a novel point mass filter (PMF) based terrain referenced navigation (TRN) by grid support adaptation and two stage filtering is proposed for computational efficiency. The inertial navigation system (INS) is one of the navigation methods based on dead reckoning and the position, velocity and attitude of the vehicle can be obtained with an inertial measurement unit (IMU) alone. INS have advantages for small short-term error, high update frequency and robustness of external disturbance, but it has a fatal disadvantage that it diverges over time due to errors of IMU output such as a bias error or white noise error [1-3]. For making up for the weakness of INS, it is integrated by using another sensor that provides absolute position or other information that can be used to estimate position such as global positioning system (GPS). INS/GPS integrated system is the most widely used integrated navigation system because it can be compensated by GPS position measurement up to INS position, velocity, attitude and bias error of IMU using Kalman filter with simple configuration [4-7]. In recently, however, jamming of spoofing which disturb the GPS information, may cause the reliability of the GPS to be lost or become unusable [8-11]. Databased referenced navigation (DBRN) is one of the alternative navigation system. The DBRN uses geophysical information that has fixed value at certain location on the earth such as gravity field [12-18] or geomagnetic field information [19-24] etc. to estimate vehicle position.

The terrain referenced navigation (TRN), which is one of the DBRN, is a navigation system suitable for INS/GPS. TRN has terrain elevation data of flight area to estimate position and uses it to perform absolute navigation [25-29]. TRN can be classified into batch processing and sequential processing. Batch processing TRN fixes the position which has the highest correlation between the terrain elevation database and measured elevation profile for a certain period of time [30-38]. Although this method has a disadvantage of heavy computation, it is useful when initial error is very large. The sequential processing TRN is a method of estimating a position through the nonlinear filter using a measurement received at every epoch. This method has an advantage that the updating period is fast and the calculation is simple, but there is a disadvantage that estimation performance is degraded or diverged when the initial error of the filter is large. In general, batch processing TRN is performed at an early stage until the position information is relatively inaccurate, and it switches to the sequential processing TRN when position information converges. In this dissertation, I considered only sequential processing.

Sequential processing TRN uses the nonlinear filter such as extended Kalman filter (EKF) [39-43], unscented Kalman filter (UKF) [42, 44-46] particle filter (PF) or point mass filter (PMF) whose measurement is the terrain elevation. In case of EKF, since the terrain elevation used in the measurement equation is not defined by a specific function, it is inevitable to perform numerical differentiation in linearizing the measurement equation. In this process, if there is large nonlinearity of the terrain, the performance of the filter may deteriorate or if may diverge in severe cases. Bayesian filters such as particle filter or point mass filter can be applied to overcome these problems [47-64]. Because Bayesian filter based TRN considers nonlinearity of measurement equation which cannot be modeled by specific equation and wide area of terrain, accurate estimates can be made and the possibility of divergence is low [67, 68]. To improve TRN performance, I apply PMF and have studied two novel approaches to improve the computation time and the estimation performance.

The first one is about the grid support adaptation. General PMF maintains a constant size of grid support which means the area where the point is set after setting the size large enough [55]. The larger the size of the grid support is, the greater the probability that a true position is presented in the grid support even though the position error is large, thus increasing the robustness of the filter. However, there is a disadvantage that the amount of calculation is increased. In addition, if the size of the grid support is large when the filter is sufficiently converged, unnecessary information is received as measurements, which may adversely affect the estimation performance of the filter. Therefore, it is advantageous for the estimation performance to appropriately change the grid support rather than fix it [55-57]. In an intuitive way, it can be used to the roughness of the terrain to change the grid support, but this does not consider the error of the measuring sensor or the multimodal that occurs in specific terrains. So, I propose a method to improve the performance of the PMF by adapting the size of the grid support according to certain conditions instead of fixing the size of the grid support uniformly considering these characteristics. At this time, the index used in the information theory called mutual information (MI) is used to determine whether the grid support is expanded or reduced.

The second one is about the two stage filtering for computation efficiency when the state variable is augmented. Generally, two- or three-dimensional state variables that are latitude and longitude, or including height are used in PMF based TRN [62]-[64]. As the dimension of state variable increases, its computation burden and its complexity exponentially increase to be implemented. To overcome this drawback, Rao-Blackwellized PMF (RBPMF), which estimates linear state variables by linear filters, has been studied by separating nonlinear state variables and linear state variables [65, 72]. However, there is a problem that the amount of computation increases exponentially in the time propagation of the linear state variable, and it has only to be solved by a heuristic method. Besides, there is a disadvantage in that a linear filter of the number of grid points must be operated. To improve this, I propose two stage PMF in this dissertation. The two stage filtering is a way to operate two filters in parallel by separating the dynamic state variable and the bias state variables [15]–[20]. The two filters are a bias free filter which estimate the dynamic state variables and a bias filter for estimating bias state variables respectively and correction is performed taking into consideration the correlation between each other. In many researches, few studies have applied different filters to these two filters. There are studies using the name “two stage” but did not succeed to the concept of the previous studies. I inherited the original two stage method and approach to benefit from applying different filters to the two filters. The main concept of the proposed algorithm is that, in PMF based TRN, the latitude and longitude that cause large nonlinearity in the measurement model are estimated by PMF, and the altitude or including velocity are estimated by using linear filter. This can greatly reduce the amount of computation and simplify the configuration, even if the state variable is further augmented rather than RBPMF.

The estimation performance is also similar to the full-state PMF.

1.2 Objectives and Contributions

The main goal of this dissertation is to improve the estimation performance and computation efficiency of the PMF based TRN by adaptation and two stage filtering technique. The contributions of this study are as follows. First, the estimation performance and the computation efficiency has improved by the grid support adaptation in PMF based TRN. Unlike general PMF based TRN that keep grid support size constant, the proposed adaptive PMF changes the size of the grid support by using MI as an adaptation index then it can consider the terrain elevation roughness and the accuracy of the measurement. As a result, the efficiency of computation has been improved by efficiently adapting the size of the grid support and eliminating the grid points of the unnecessary area, and the estimation performance also has been improved by excluding unnecessary measurement.

Second, the computation efficiency has been improved by TSPMF when the more state variables are augmented. The most intuitive way to improve the performance of a PMF based TRN is to estimate more state variables. However, in the case of PMF, the more state variables, the more exponential the computation burden is. There is RBPMF as a pre-invented method for solving this problem, but it has a drawback that it needs to drive Kalman filters as many as the number of grid points. The proposed TSPMF can estimate nonlinear state variables by general PMF and linear state variables by only one Kalman filter separately. At this time, the correlation nonlinear state variables and linear state variables is considered by some coupling equations. The simulations has been performed for full state PMF, RBPMF and TSPMF to verify improvement by using the proposed method, as a result, TSPMF has had the most efficiency for computation burden and it has shown almost same performance of the full state PMF which is the most optimal filter among them.

1.3 Organization of the Dissertation

Chapter 1 provides the motivation and background of this dissertation as well the objective and contributions. In Chapter 2, detailed information to understand the main contributions of this dissertation is provided including nonlinear filters, and typical sequential processing TRN algorithms. Chapter 3 describes the grid design method for the PMF. The conventional grid design methods proposed by

Bergman and Simandl are explained. Also, the new grid design method considering model uncertainties is described in detail and it is shown that the novelty of the proposed grid design by the PTRN simulations. Chapter 4 provides detailed derivation of a modified measurement model for slant range measurement. It is shown how to reflect on horizontal and vertical distance to the measurement model caused by the slant range. Also, the influence of the vehicle attitude and the measurement angle to the slant range is separated and measurement variance that reflects the attitude errors and the measurement angle errors is proposed. Chapter 5 gives conclusions.

Chapter 2

Point Mass Filter Based Terrain Referenced Navigation

This chapter presents an introduction to the general PMF based TRN. The TRN is based on strapdown INS (SDINS) and it uses terrain information as an aided measurement. Therefore, this chapter briefly describes SDINS first. Next, a general PMF based TRN will be described.

2.1 Strapdown Inertial Navigation System

The INS is one of the navigation system which is based on dead reckoning with inertial measurement unit (IMU) composed of accelerometer and gyroscope. Early INS used platform with gimbaled IMU but it is inevitable to mechanical complexity, heavy weight and large room. Now a day, gimbaled IMUs are rarely used because of these drawbacks and SDINS is widely used because of its benefits which are lower cost and reduced size. The SDINS is needed more complex calculation process that gimbaled INS but it is not a problem for computational capacity of computers these days. The INS mentioned later means SDINS, the coordinate represents and INS algorithm will be explained to explain the concept of INS.

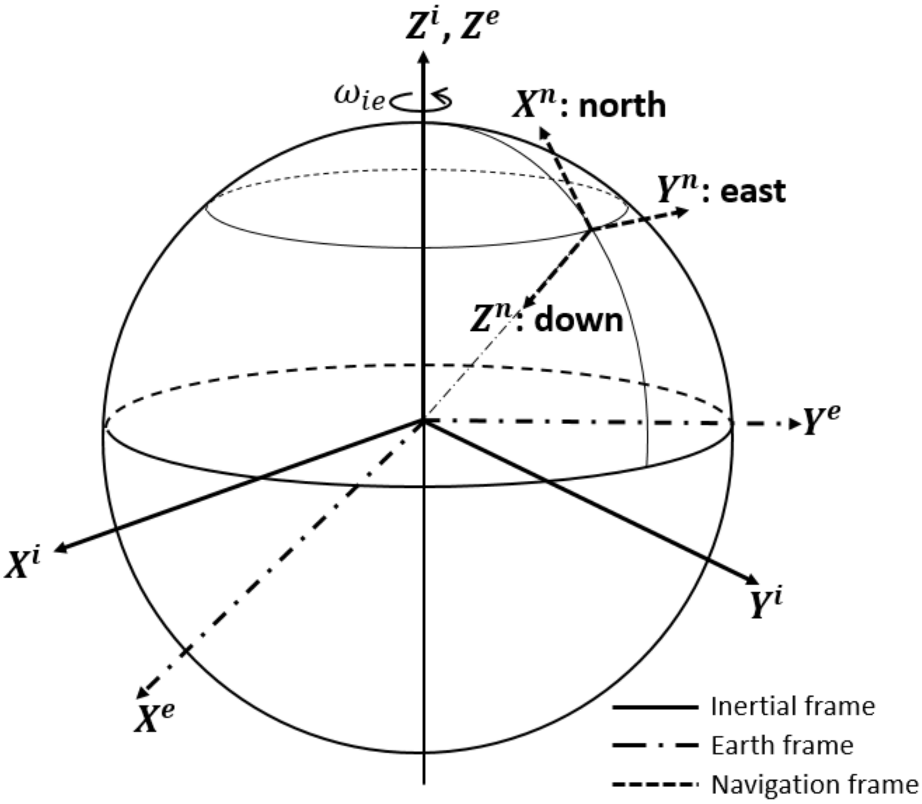

Figure 2.1 Reference frames

2.1.1 Reference Frames

The reference frames are important to understanding INS algorithm. For the navigation on the Earth, it must be defined to a set of axes so that inertial measurements can be associated with the navigation solution for the Earth. In the navigation, the reference frame is a standard for expressing navigation information. In this section, inertial frame, Earth frame, navigation frame and body frame are resented. Figure 2.1 shows reference frames.

- **Inertial frame**

The inertial frame is a standard coordinate that is the basis of the law of physics. The center of the coordinate and the z-axis coincide with the center of the Earth and the axis of rotation of the Earth, and the x-axis faces the mean vernal equinox. So, it is also called by Earth fixed inertial (ECI) frame. This frame cannot be said to be stopped strictly speaking, but it can be assumed that there are no rotation and acceleration because it is very slow compared to the Earth's physical time. The inertial frame, denoted by the symbol i as Fig. 2.1, is the most important frame for the understanding of INS because IMU, a sensor for INS, measures the acceleration or rotation of a vehicle based on inertial frame.

- **Earth frame**

In the Earth frame, the Earth centered Earth fixed (ECEF) is most widely used as an Earth frame. The ECEF is quite similar to the ECI frame. In ECEF, the center and z-axis of the coordinate coincides with the center of the Earth and the Earth rotation axis, like the ECI frame, and rotates with the Earth rotation. So, if the IMU is stopped, the centripetal acceleration due to the Earth rotation will be measured on the accelerometer and the angular velocity about the earth's rotational axis will be measured in the gyroscope. At this time, the x-axis is facing the Greenwich Observatory and this position becomes the starting point of the longitude. Here is 0 degree and it increases in the east or west direction. The latitude is relative to the equator, defined as 90 degrees for north and 90 degrees for south. It is a very important coordinate because it expresses the position based on the ECEF when performing navigation on the Earth in general. It is denoted by the symbol e as Fig. 2.1.

- **Navigation frame**

The navigation frame is a coordinate based on the local level plane at the Earth's surface relative to the current position of the vehicle. The axes face north, east and down direction, or east, north and up, respectively. When we define the velocity of the vehicle, the velocity can be defined in the navigation frame because it is ambiguous to define the direction and the unit in the Earth frame. When performing dead reckoning using this velocity, the position is calculated by geometric transformation. It is also used as a reference frame to define the attitude of the vehicle. It is denoted by the symbol n as Fig. 2.1.

- **Body frame**

The body frame refers to a coordinate fixed to the body to define the attitude of the vehicle, which is generally defined by its axes are defined by engineers. In case of INS, the body frame is used to be defined as the sensor frame for convenience. The three axes are generally defined as forward, right and down. The attitude of the vehicle is defined by relationships between body frame and navigation frame. The measurement of the INS from the IMU are measured on this frame. It is denoted by the symbol b as Fig. 2.2

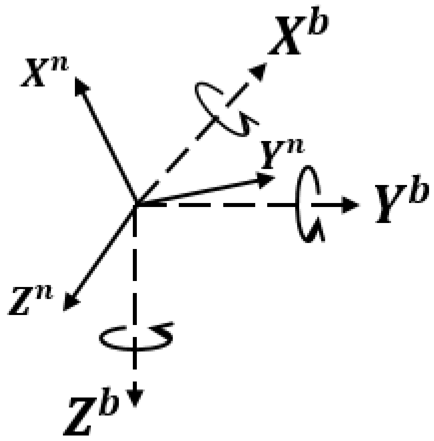

Figure 2.2   Body frame representation

2.1.2 Inertial Navigation Mechanization

The INS is widely used because of its accuracy, high sampling rate, robustness to external disturbance and self-positioning. INS does not need any additional aid and only uses IMU for calculating position, velocity and attitude of the vehicle. The IMU consisted of accelerometer and gyroscope is able to measure the specific force and angular rate between body frame and inertial frame of the vehicle. So, we should understand exactly the output of the IMU. In this section, it will be explained about output of the IMU and the way to treat that for calculating navigation solutions by SDINS mechanization.

2.1.2.1 Outputs of Inertial Measurement Unit

The accelerometer measures a specific force of the vehicle between inertial frame and body frame. The specific force is the combination of the acceleration due to maneuver $\mathbf{a}_i$, and the acceleration due to the gravitational field $\mathbf{g}_m$ in the inertial coordinate system. Therefore, the accelerometer measures specific force $\mathbf{f}$ as follows

$$\mathbf{f} = \mathbf{a}_i - \mathbf{g}_m . \tag{2.1}$$

The inertial acceleration is the second derivative of the position vector r with respect to time in the inertial space. So, the inertial acceleration is expressed as follow

$$\mathbf{a}_i = \left. \frac{d^2\mathbf{r}}{dt^2} \right|_i . \tag{2.2}$$

where i in subscript means observation in the inertial frame.

If the vehicle is rotating with the Earth rotation, it is expressed in centripetal acceleration in the inertial frame. In other words, besides the gravity due to universal gravitation, the centripetal acceleration due to the earth rotation also acts as gravity. This gravity is called by plum-bob gravity and expressed as follow

$$\mathbf{g} = \mathbf{g}_m - \boldsymbol{\omega}_{ie} \times (\boldsymbol{\omega}_{ie} \times \mathbf{r}). \tag{2.3}$$

$$\boldsymbol{\omega}_{ie} = \begin{bmatrix} 0 & 0 & \Omega_{ie} \end{bmatrix}^T \tag{2.4}$$

where $\boldsymbol{\omega}_{ie}$ is the Earth rotation vector, Ω_{ie} is the angular rate of the Earth. Subscript ie means relative physical quantities between the inertial frame and Earth frame.

Substituting from (2.2) and (2.3) into (2.1) yields the specific force measured by accelerometer as follow

$$\mathbf{f} = \frac{d^2\mathbf{r}}{dt^2} - \mathbf{g} + \boldsymbol{\omega}_{ie} \times (\boldsymbol{\omega}_{ie} \times \mathbf{r}). \tag{2.5}$$

The gyroscope in the IMU senses an angular rate of the vehicle when it is turning. The angular rate is the relative angular rate between the inertial frame and the body frame. Therefore, the gyroscope not only measures the angular rate caused by the maneuver between the navigation frame and the body frame $\boldsymbol{\omega}_{nb}$, but also measures the angular rate caused by the Earth's rotation $\boldsymbol{\omega}_{ie}$ and transport rate $\boldsymbol{\omega}_{en}$ which is generated by moving the curved surface of the Earth. The measured angular rate $\boldsymbol{\omega}_{ib}$ is expressed by

$$\boldsymbol{\omega}_{ib}^b = \boldsymbol{\omega}_{ie}^b + \boldsymbol{\omega}_{en}^b + \boldsymbol{\omega}_{nb}^b \tag{2.6}$$

where superscript b means that it is measured in the body coordinate system. Since the attitude is calculated using the relative angular rate between the body frame and the navigation frame $\boldsymbol{\omega}_{nb}$, it is necessary to remove $\boldsymbol{\omega}_{ie}^{b}$, which is determined by the position, and $\boldsymbol{\omega}_{en}^{b}$, which is determined by velocity in the output of the gyroscope.

2.1.2.2 Attitude update equation

The attitude update equation, which uses angular rate between navigation frame and body frame and previously known attitude, follows well known attitude kinematics equations. The representation by direction cosine matrix (DCM) as follows

$$\dot{\mathbf{C}}_b^n = \mathbf{C}_b^n \left(\boldsymbol{\omega}_{nb}^{b} \times \right) \tag{2.7}$$

$$\boldsymbol{\omega}_{nb}^{b} = \boldsymbol{\omega}_{ib}^{b} - \mathbf{C}_n^b \left(\boldsymbol{\omega}_{en}^{n} + \boldsymbol{\omega}_{ie}^{n} \right) \tag{2.8}$$

The angular rate between inertial and body frame $\boldsymbol{\omega}_{ib}^{b}$ can be measured gyroscope, the Earth rotation rate in local position $\boldsymbol{\omega}_{ie}^{n}$ can be obtained as follow

$$\boldsymbol{\omega}_{ie}^{n} = \left[\omega_{ie} \cos L \quad 0 \quad -\omega_{ie} \sin L \right]^{T} . \tag{2.9}$$

The transport rate $\boldsymbol{\omega}_{en}^{n}$ is defined by a velocity and position of the vehicle, and can be expressed as

$$\boldsymbol{\omega}_{en}^{n} = \begin{bmatrix} \dfrac{v_E}{R_0 + h} & \dfrac{-v_N}{R_0 + h} & \dfrac{-v_E \tan L}{R_0 + h} \end{bmatrix} \tag{2.10}$$

where R_0 is the radius of the Earth, h is height of the vehicle, L is the latitude, v_N and v_E are velocity of the north and east direction, respectively.

2.1.2.3 Velocity and Position Update

The velocity of the vehicle is required to calculate with respect to ground. The inertial velocity $\left.\dfrac{d\mathbf{r}}{dt}\right|_i$ is represented to ground velocity using the Coriolis equation

$$\left.\frac{d\mathbf{r}}{dt}\right|_i = \left.\frac{d\mathbf{r}}{dt}\right|_e + \boldsymbol{\omega}_{ie} \times \mathbf{r} \tag{2.11}$$

The first term of (2.11) right hand side is the ground velocity $\mathbf{v}_e$ of the vehicle and the acceleration on the inertial frame can be obtained by differentiating (2.11) as follows

$$
\begin{aligned}
\left.\frac{d^2\mathbf{r}}{dt^2}\right|_i &= \left.\frac{d\mathbf{v}_e}{dt}\right|_i + \boldsymbol{\omega}_{ie} \times \left.\frac{d\mathbf{r}}{dt}\right|_i \\
&= \left.\frac{d\mathbf{v}_e}{dt}\right|_n + \left(\boldsymbol{\omega}_{in}^n + \boldsymbol{\omega}_{ie}^n\right) \times \mathbf{v}_e + \boldsymbol{\omega}_{ie}^n \times \left(\boldsymbol{\omega}_{ie}^n \times \mathbf{r}\right)
\end{aligned}
\tag{2.12}
$$

The specific force $\mathbf{f}^b$ is measured by the accelerometer as (2.5), then the acceleration equation can be derived from (2.12)

$$
\dot{\mathbf{v}}^n = \mathbf{C}_b^n \mathbf{f}^b - \left(2\boldsymbol{\omega}_{ie}^n + \boldsymbol{\omega}_{en}^n\right) \times \mathbf{v}^n + \mathbf{g} \tag{2.13}
$$

where, the superscripts mean the frame where each vector is expressed, and $\mathbf{v}^n$ is the velocity vector on the navigation frame as $\mathbf{v}^n = \begin{bmatrix} v_N & v_E & v_D \end{bmatrix}^T$. The velocity on the navigation frame is computed by integration of the (2.22). The position which are latitude, longitude and height of the vehicle can be calculated as follows

$$
\dot{L} = \frac{v_N}{R_o + h} \tag{2.14a}
$$

$$
\dot{l} = \frac{v_E}{\left(R_o + h\right)\cos l} \tag{2.14b}
$$

$$
\dot{h} = -v_D \tag{2.14c}
$$

The overall INS process is shown in Fig. 2.3.

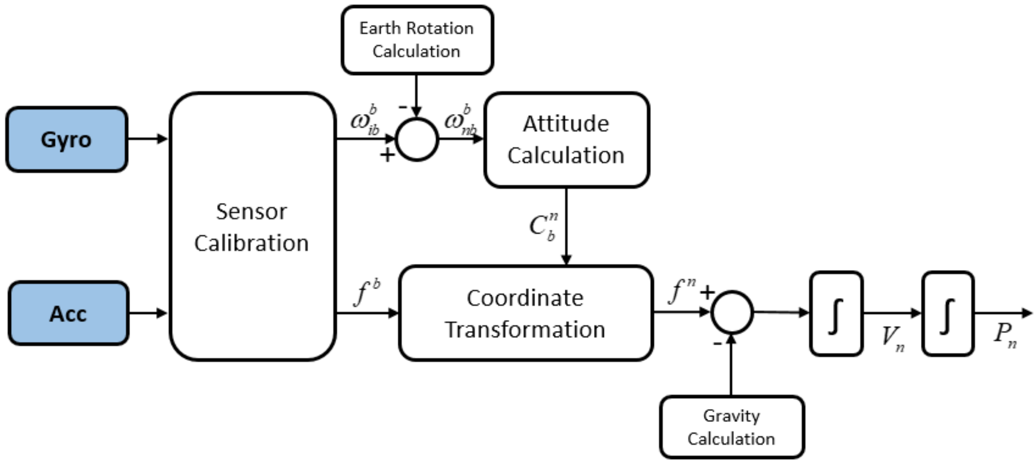

Figure 2.3 Strapdown INS algorithm

2.1.3 INS Error Propagation

Since the position of the INS is obtained from the IMU output through coordinate transformation and integration, the position error is affected not only by the velocity error but also by the attitude error, the accelerometer and the gyro error. Table 2.1 shows the error elements affecting the position error in the north direction of the inertial navigation system and the position error in the north direction caused by each error elements. The medium term error is an error model considering 84.4 minutes of error propagation period of the inertial navigation system. The short term error is an error model for a short time within 1/4 of the

Schuler cycle.

From Table 2.1, the elements and sizes of the inertial navigation system are assumed as shown in Table 2.2 to observe the positional errors over time. The medium term position error due to the error factors in Table 2.2 is shown in Fig. 2.4. In Fig. 2.4, total error is calculated by RSS (root sum square) as shown in Equation (2.1). As shown in Fig. 2.4, the east position error and the north accelerometer bias error are major factors of the position error up to about 2500 seconds, which is half of the Schuler cycle, and the influence of the east gyro bias error and the vertical axis attitude error is dominant. In the relation between the error of the inertial sensor and the navigation error, the horizontal axis position error is mainly influenced by the bias error of the accelerometer, and the vertical axis position error is mainly influenced by the gyro bias error. And the long - term position error is a major factor in error related gyroscope.

Table 2.1 INS position errors according to error elements

Error element	Medium Term Error	Short Term Error
Initial velocity error (δv_N)	$\left(\dfrac{\sin\omega_s t}{\omega_s}\right)\delta v_N$	$\delta v_N t$
Initial east tilt error (φ_E)	$R_0\left(1-\cos\omega_s t\right)\varphi_E$	$\dfrac{1}{2}g\varphi_E t^2$
North accelerometer bias(∇_N)	$\left(\dfrac{1-\cos\omega_s t}{\omega_s^2}\right)\nabla_N$	$\dfrac{1}{2}\nabla_N t^2$
Initial vertical tilt error (φ_D)	$R_0\omega_N\left(t-\dfrac{\sin\omega_s t}{\omega_s}\right)\varphi_D$	$\dfrac{1}{6}g\omega_N\varphi_D t^3$
East gyro bias (ε_E)	$R_0\left(t-\dfrac{\sin\omega_s t}{\omega_s}\right)\varepsilon_E$	$\dfrac{1}{6}g\varepsilon_E t^3$
Vertical gyro bias (ε_D)	$-R_0\omega_N\left(\dfrac{t^2}{2}-\dfrac{1-\cos\omega_s t}{\omega_s^2}\right)\varepsilon$	$\dfrac{1}{6}g\omega_N\varepsilon_D t^4$

* $\omega_s=\sqrt{\dfrac{g}{R_0}}$: Schuler frequency,

Table 2.2 Error elements and its values

Error element	Value
Initial velocity error (δv_N)	0.01m/s
Initial east tilt error (φ_E)	0.11mrad
North accelerometer bias(∇_N)	100µg
Initial vertical tilt error (φ_D)	1mrad
East gyro bias (ε_E)	0.01deg/hr
Vertical gyro bias (ε_D)	0.01deg/hr

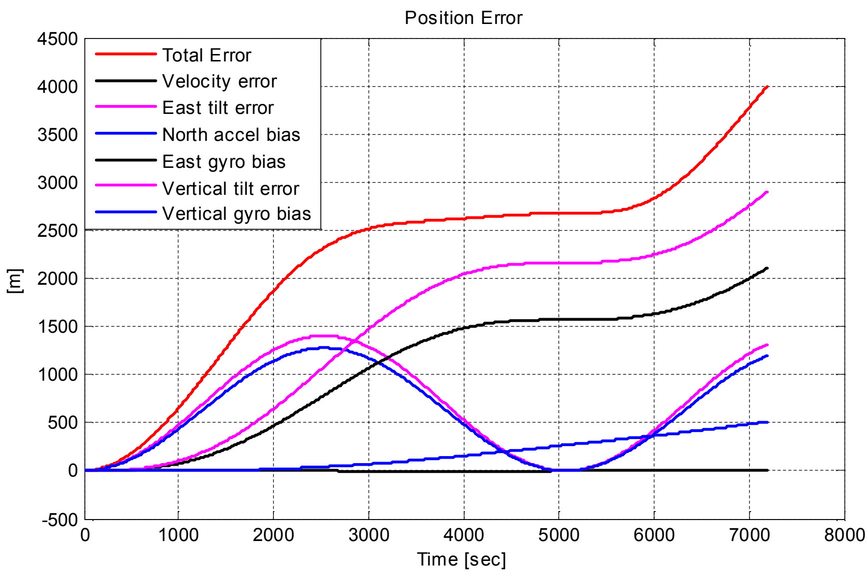

Figure 2.4 Medium term INS position error caused by error elements

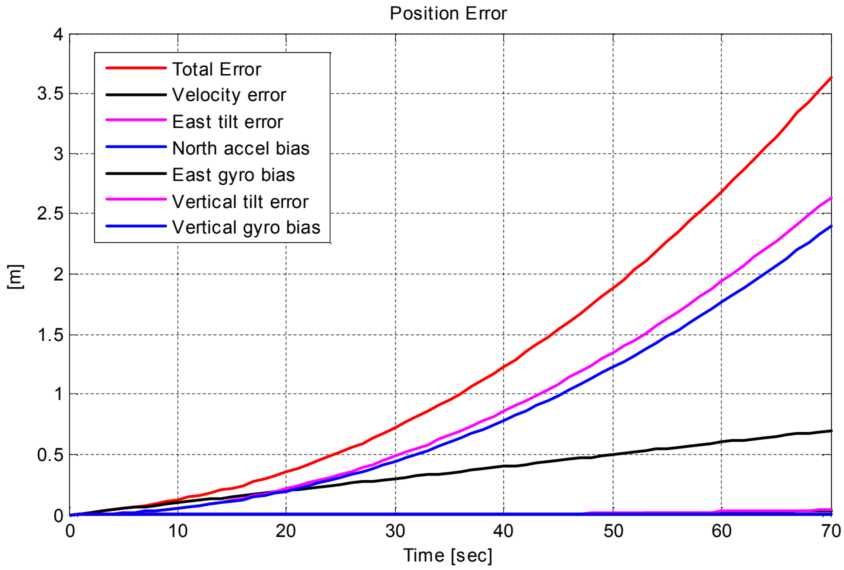

Figure 2.5 Short term INS position error caused by error elements

2.2 Terrain Referenced Navigation

In this section, it is described that the navigation components and their characteristics for performing the TRN and how they are reflected in the TRN. In addition, the nonlinear filtering methods described in Section 2.2 are applied to the TRN and the numerical simulation results are introduced.

2.2.1 General PMF Algorithm

The Bayesian filter is a technique for obtaining the probability density function of the state variable $\mathbf{x}_k$ with respect to the measurement $\mathbf{Z}^k$, and the following nonlinear system and measurement model are considered.

$$\mathbf{x}_{k+1} = \mathbf{f}_k\left(\mathbf{x}_k\right) + \mathbf{w}_k \tag{2.15}$$

$$\mathbf{z}_k = \mathbf{h}_k\left(\mathbf{x}_k\right) + \mathbf{v}_k \tag{2.16}$$

where $\mathbf{f}_k\left(\cdot\right)$ is the nonlinear system model, $\mathbf{h}_k\left(\cdot\right)$ is the nonlinear measurement model, $\mathbf{w}_k$ and $\mathbf{v}_k$ are additive white noise errors of system and measurement model with known probability density functions $p\left(\mathbf{w}_k\right)$, $p\left(\mathbf{v}_k\right)$, respectively.

A posterior probability density function (pdf) $p\left(\mathbf{x}_k \middle| \mathbf{Z}^k\right)$ which is purpose of the Bayesian filter can be calculated as follows:

$$p\left(\mathbf{x}_k \middle| \mathbf{Z}^k\right) = \frac{p\left(\mathbf{x}_k \middle| \mathbf{Z}^{k-1}\right) p\left(\mathbf{z}_k \middle| \mathbf{x}_k, \mathbf{Z}^k\right)}{p\left(\mathbf{z}_k \middle| \mathbf{Z}^{k-1}\right)} \tag{2.17}$$

where $p\left(\mathbf{x}_k \middle| \mathbf{Z}^{k-1}\right)$ is a prior pdf, $p\left(\mathbf{z}_k \middle| \mathbf{x}_k, \mathbf{Z}^k\right)$ is a likelihood function and $p\left(\mathbf{z}_k \middle| \mathbf{Z}^{k-1}\right)$ is normalization constant. Each terms can be expressed as follows:

$$p\left(\mathbf{x}_k \middle| \mathbf{Z}^{k-1}\right) = \int p\left(\mathbf{x}_{k-1} \middle| \mathbf{Z}^{k-1}\right) p\left(\mathbf{x}_k \middle| \mathbf{x}_{k-1}\right) d\mathbf{x}_{k-1} \tag{2.18}$$

$$p\left(\mathbf{z}_k \middle| \mathbf{x}_k, \mathbf{Z}^k\right) = p_{\mathbf{v}_k}\left(\mathbf{z}_k - \mathbf{h}_k\left(\mathbf{x}_k\right)\right) \tag{2.19}$$

$$p\left(\mathbf{z}_k \middle| \mathbf{Z}^{k-1}\right) = \int p\left(\mathbf{x}_k \middle| \mathbf{Z}^{k-1}\right) p\left(\mathbf{z}_k \middle| \mathbf{x}_k\right) d\mathbf{x}_k \tag{2.20}$$

where (2.18) is the well-known Chapman-Kolmogorov expression and $p\left(\mathbf{x}_k \middle| \mathbf{x}_{k-1}\right)$ is the transition density determined by the system model.

As can be seen from (2.18), integral operation must be perform for obtaining a posterior pdf $p\left(\mathbf{x}_k \middle| \mathbf{Z}^k\right)$. However, the analytical solution can be obtained with special assumption that the system model and the measurement model are linear and each pdf are additive, independent and Gaussian. PMF performs numerical integration on (2.18) and (2.20), assuming these assumptions are not satisfied. The

PMF algorithm represents pdf by grid of points, by set of area masses of each grid point's neighborhood, and by set of pdf values at the grid points. The general algorithm of the PMF is as follows.

1) Initialization

Set an initial grid $\Xi_0(N_0)$ for the prior pdf $p(\mathbf{x}_0)$.

2) Time propagation of grid points

Propagate the grid $\Xi_k(N_k)$ to $H_{k+1}(N_k)=\{\boldsymbol{\eta}_{k+1,i};i=1,\cdots,N_k\}$, by the system dynamic model $\boldsymbol{\eta}_{k+1,i}=\mathbf{f}_k(\boldsymbol{\xi}_{k,i})$, where $\boldsymbol{\eta}$ is a set of the propagated grid points and $\boldsymbol{\xi}$ is a set of the prior defined grid points. k is a time index and i is an index of points.

3) Grid redefinition

Redefine the propagated grid $H_{k+1}(N_k)$ to a new grid $\Xi_{k+1}(N_{k+1})$ with the same structural properties as the original grid $\Xi_{k+1}(N_{k+1})=\{\boldsymbol{\xi}_{k+1,j};j=1,\cdots,N_{k+1}\}$. Then, compute the volume pass of the neighborhood $\mathrm{D}_{k+1}(N_{k+1})=\{\Delta\boldsymbol{\xi}_{k+1,j};j=1,\cdots,N_{k+1}\}$.

4) Prediction

Compute the a prior pdf at the new grid $\Xi_{k+1}(N_{k+1})$, by using

$$P_{k+1|k,j} = \sum_{i=1}^{N_k} \Delta\xi_{k+1,i} P_{k|k,i} p_{\mathbf{w}_k}\left(\xi_{k+1,i} - \boldsymbol{\eta}_{k+1,i}\right) \quad \text{for} \quad j = 1,\cdots,N_{k+1}.$$

5) Filtering

Compute the posterior pdf at the new grid $\Xi_{k+1}\left(N_{k+1}\right)$ for $j = 1,\cdots,N_{k+1}$ by $P_{k+1|k+1,i} = c_k^{-1} P_{k+1|k,i} p_{\mathbf{v}_k}\left(\mathbf{z}_k - \mathbf{h}_k\left(\xi_{k+1,i}\right)\right)$ where $c_k = \sum_{i=1}^{N_{k+1}} \Delta\xi_{k+1,i} P_{k+1|k,i} \cdot p_{\mathbf{v}_k}\left(\mathbf{z}_k - \mathbf{h}_k\left(\xi_{k+1,i}\right)\right)$. Then, calculate the minimum mean square error estimate, $\hat{\mathbf{x}}_{k+1} = \sum_{i=1}^{N_{k+1}} \xi_{k+1,i} P_{k+1|k+1} \Delta\xi_{k+1,i}$

Figure. 6 presents the general PMF algorithm by block diagram.

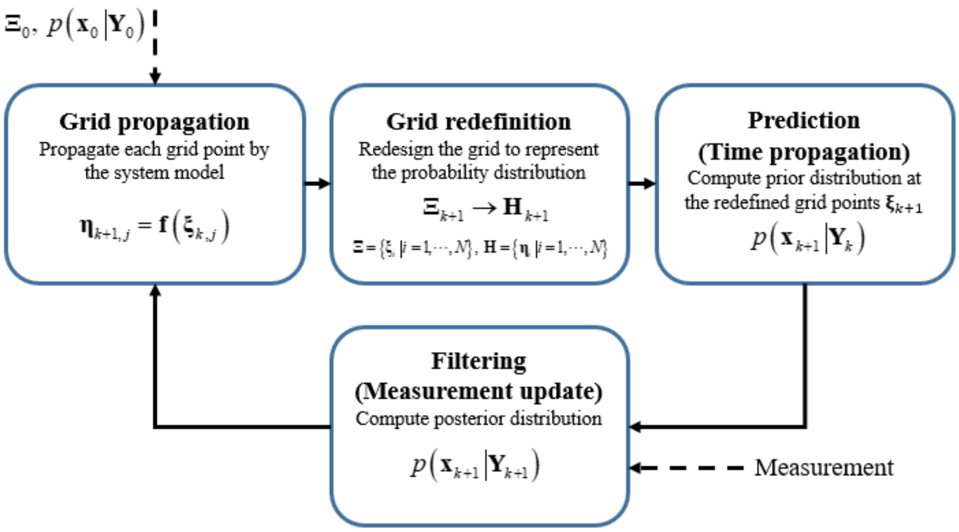

Figure 2.6 General PMF algorithm

2.2.2 Point Mass Filter Based TRN

Sequential processing TRN uses the difference between measured terrain elevation and the database terrain elevation as measurement of the filter. Because the measurement equation is determined by the terrain which cannot be represented by specific function, we should use EKF with numerical derivatives or Bayesian filter with numerical integration. The EKF has the disadvantage that the nonlinearity is severe of the initial error is very large. So, we apply the PMF to TRN which has robustness for the terrain nonlinearity and large initial error. The system model and the measurement model for the PMF based TRN are given as follows:

$$\mathbf{x}_{k+1} = \mathbf{x}_k + \mathbf{u}_k dt + \mathbf{w}_k \tag{2.21}$$

$$z_k = h(\mathbf{x}_k) + v_k \tag{2.22}$$

where $\mathbf{x}_k$ is the horizontal position of the vehicle, $\mathbf{u}_k$ is velocity vector obtained by INS, dt is sampling time and $\mathbf{w}_k$ is the additive white process noise error. $\mathbf{z}_k$ is the terrain elevation measurement, $h(\cdot)$ is the measurement equation determined by terrain elevation and $\mathbf{v}_k$ is the additive white measurement noise error. The measurement model $h(\mathbf{x}_k)$ is expressed by as follows

$$h(\mathbf{x}_k) = -h_{DB}(L_k, l_k) + h_k \tag{2.23}$$

where $h_{DB}(L_k, l_k)$ is a terrain elevation obtained from DEM with respect to latitude and longitude, h_k is a height of the vehicle. As can be seen in (2.23), it can be known that the measurement is a range from ground to vehicle. Figure. 2.7 shows the geometry of the measurement.

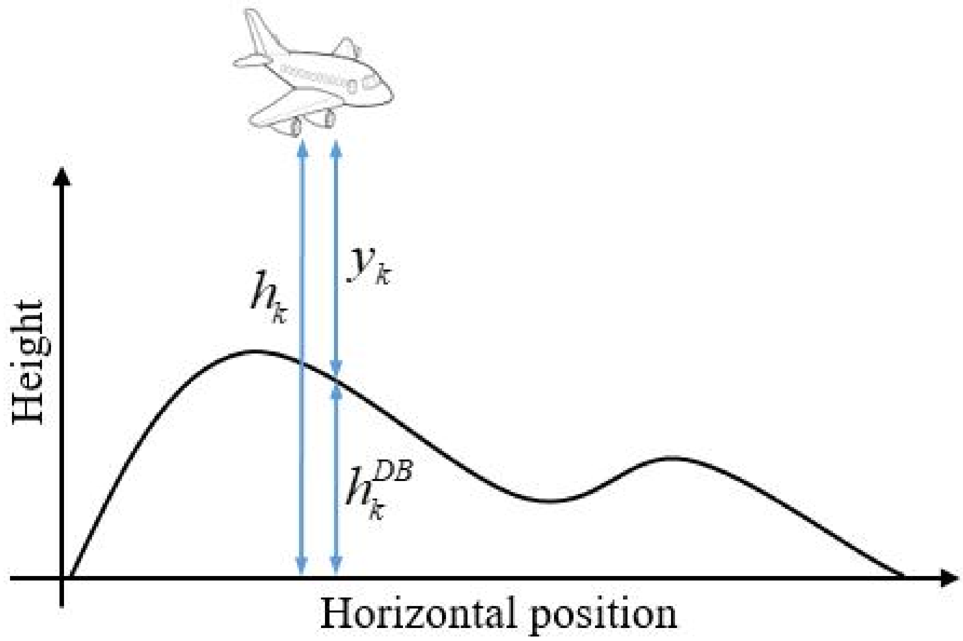

Figure 2.7   Measurement of the TRN

In general, the integrated navigation system combined with INS uses 15 state variables that consist of position, velocity, attitude and IMU bias error. However, in the case of PMF, since the amount of computation increases exponentially according to the number of state variables, only latitude and longitude are set as state variables. In case of aerial application which is considered in this paper, terrain elevation measurement $\mathbf{z}_k$ can be obtained by difference between the absolute altitude obtained by the barometric altimeter and the distance between the vehicle and the ground obtained by the RADAR. And it is assumed that the error between the barometric altimeter and the RADAR is Gaussian and independent of each other.

Chapter 3

Grid Support Adaptation Using Mutual Information

Measurements of TRN use the difference between the measured terrain elevation and the database's terrain elevation. Therefore, the measurement equation should be a terrain elevation according to the position of the vehicle. If the terrain itself cannot be defined as a specific function, then the nonlinearity is very strong. Therefore, one of the Bayesian filters, PMF, is widely used for terrain reference navigation. In PMF, the estimation performance is changed by several setting parameters. In this chapter, I analyzed the relationship between the performance and grid support, one of the configuration parameters, and grid support and measurement quality. In addition, an index that determines the quality of the measurement has been set and applied to the grid support adaptation technique.

3.1 Grid Support Adaptation Algorithm

In this section, it is necessary to first define the quality of the measurement., because the proposed adaptation rule is based on determination for measurement quality. Therefore, I will first discuss the quality of the measurements in accordance with the grid support, and then discuss how to determine the quality of the measurements and how to adapt the grid support using the measurement quality.

3.1.1 Measurement Quality According to Grid Support

PMF is a grid based Bayesian filter and its performance is determined by grid design parameter such as grid support, resolution and etc. The grid support, in general, is set widely to express the integral approximation of (2.15) as accurately as possible. In other words, the larger the grid support is, the more reliable the measurement equation is represented, and conversely, the smaller the grid support, the less reliable the measurement equation. Therefore, it can be expected that the wider the grid support, the better the estimation performance of the filter. However, this logic may not always be appropriate in PMF based TRN.

I would like to think of two cases of this problem. First, let’s assume that the filter is sufficiently converged. In this case, if the grid support is set too wide, positions with the same elevation as the actual terrain elevation can exist in many points in the grid support. Therefore, peaks of the likelihood can occur in many points, and the estimation performance may be degraded because the likelihood can make it more imprecise by updating the prior pdf to the posterior pdf. In other words, the wider the grid support, the more accurate the measurement equation can be, but the lower the quality of the measurement. Second, let's assume that the estimation error is too large. In this case, if the size of the grid support is not large enough to contain the actual position, the filter may diverge. This can be the case when the initial error is very large, or when the error is getting large as the vehicle encounter continuous flat terrain area. Based on these cases, widening the grid support to accurately represent the measurement equation does not always guarantee the quality of the measurement. In conclusion, in order to improve the estimation performance, it may be advantageous to change the size of the grid support in consideration of the quality of the measurement.

3.1.2 Mutual Information for Measurement Quality Discrimination

As the mention in the previous sub-section, the grid support adaptation considering quality of the measurement can improve estimation performance. In an intuitive way, we can consider the measurement quality by taking into account the roughness of the terrain. For example, σ_T or σ_Z [26] which is generally a way to calculate the roughness of the terrain can be used. If the terrain is rough, it can be judged that the measurement quality is good. On the contrary, if the terrain is flat, the measurement quality is considered badly. However, considering only the roughness of the terrain, the error of the measurement sensor, such as RADAR or barometric altimeter, cannot be taken into consideration and the multimodality of the pdf in a specific terrain cannot be considered. To overcome these problem, we propose a method to identify measurement quality by MI. MI is an index used in information theory and is an index of how the information between two random variables is correlated [29]. If MI is large, it means that two random variables are closely related to each other. On the other hand, if it is small or smaller than 0, it means that there is no relationship between two random variables. The MI for two random variables X and Y can be expressed as (3.1), which is expressed as the entropy of each random variable.

$$
\begin{aligned}
I(X;Y) &= \sum_{x,y} p(x,y)\log\frac{p(x,y)}{p(x)p(y)} \\
&= H(X) - H(X|Y) \\
&= H(Y) - H(Y|X)
\end{aligned}
\tag{3.1}
$$

where $I(X;Y)$ is MI of X and Y, $H(\cdot)$ is entropy which can be calculated by

$$
H(X) = -\sum_{i} X_i \log(X_i) \tag{3.2}
$$

where X_i is a i-th component of pdf $p(X)$. To determine the measurement quality using this index, set X to $\mathbf{x}|\mathbf{Z}^{k-1}$ and Y to $\mathbf{z}_k|\mathbf{Z}^{k-1}$ then (3.1) can be written as follow.

$$I\left(\mathbf{x}\middle|\mathbf{Z}^{k-1};\mathbf{z}_k\middle|\mathbf{Z}^{k-1}\right)=H\left(\mathbf{x}\middle|\mathbf{Z}^{k-1}\right)-H\left(\mathbf{x}\middle|\mathbf{Z}^{k-1}\middle|\mathbf{z}_k\middle|\mathbf{Z}^{k-1}\right) \tag{3.3}$$

In this case, $\mathbf{z}_k|\mathbf{Z}^{k-1}$ can be expressed $\mathbf{z}_k$ because the measurement is independent of every epoch. Therefore, (3.3) can be derived as follows

$$\begin{aligned}I\left(\mathbf{x}\middle|\mathbf{Z}^{k-1};\mathbf{z}_k\middle|\mathbf{Z}^{k-1}\right)&=H\left(\mathbf{x}_k\middle|\mathbf{Z}^{k-1}\right)-H\left(\mathbf{x}_k\middle|\mathbf{Z}^{k-1}\middle|\mathbf{z}_k\right)\\&=H\left(\mathbf{x}_k\middle|\mathbf{Z}^{k-1}\right)-H\left(\mathbf{x}_k\middle|\mathbf{Z}^{k}\right)\end{aligned} \tag{3.4}$$

From (11), we can see that the MI of $\mathbf{x}|\mathbf{Z}^{k-1}$ and $\mathbf{z}_k|\mathbf{Z}^{k-1}$ is the entropy difference between the prior and posterior probability distributions.

Now, let's look at the physical meaning of equation (3.4). In left side of equation (3.4), the MI is an index of how the MI of $\mathbf{x}|\mathbf{Z}^{k-1}$ and $\mathbf{z}_k|\mathbf{Z}^{k-1}$ is, that is, how the measurement $\mathbf{z}_k$ is related to $\mathbf{x}|\mathbf{Z}^{k-1}$. Therefore, if it is larger than 0, it can be considered that a good measurement has come in. Conversely, if it is smaller than or equal to 0, it can be considered that a bad measurement has been received. Likewise, let's look at the meaning of the right side in (3.4). The entropy of the prior and posterior estimate indicate how the pdf is concentrated in one place. In other words, they are related to their variance. Therefore, if the filter performs a measurement update with good measurements coming in, the entropy of the posterior will be smaller than the entropy of the prior. Conversely, if it is less than 0, it means that the posterior pdf is wider than the prior pdf, which has the same meaning as the left side. According to [79], entropy is also used as an index to determine the uncertainty of a random variable, which supports the validity of determining the quality of a measurement by the difference of entropy between prior and posterior pdf. Some readers can think intuitively that using variance or standard deviation will have the same effect instead of entropy. But, in case of non-Gaussian, it can be calculated that the variance is larger in the more concentrated probability distribution (see section 3.1.2.1). Thus, the entropy is more advantageous than variance when determining the concentration of a non-Gaussian probability distribution.

3.1.2.1 Comparison Variance and MI for Discriminator About Measurement Quality

Suppose normalized pdf A and B as following equation and figure.

$$\begin{aligned} p(A) &= N\left(0,1^2\right) \\ p(B) &= N\left(0,1^2\right)+N\left(1.5,0.3^2\right) \end{aligned} \tag{3.5}$$

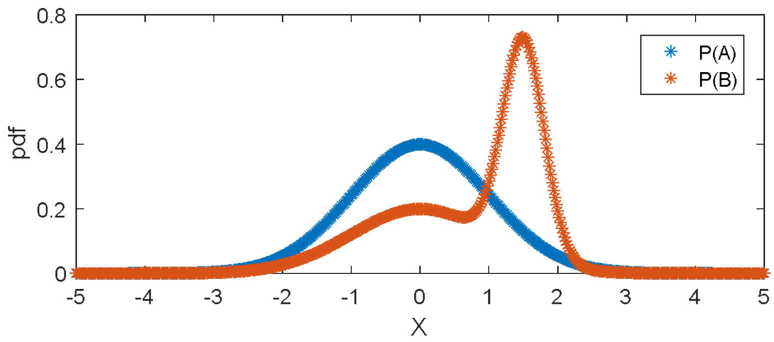

Figure 3.1 Normalized pdf of A and B

In above figure, the peak of pdf B is formed narrower and higher than that of pdf A. Therefore, it can be said that a good quality measurement is obtained if A is prior and B is posterior pdf in PMF. At this time, the standard deviations of A and B are 1 and 1.05, respectively. This means that the pdf is inaccurate by measurement, and this is a result that does not reflect the shape of the pdf because the pdfs are not normal distribution. However, when we calculate the MI, it has a positive value of 0.16. This means that the posterior pdf is more concentrated in one place and it is more accurate. For this reason, MI is an index that better describes the shape of the pdf than the standard deviation or variance. So, we have used MI as a judging index for the quality of the measurement.

3.1.3 Adaptation Algorithm

In case of PMF based TRN, posterior pdf is obtained by multiplying prior pdf by likelihood. The likelihood is determined by the shape of the terrain and the measurement error. After all, MI considers likelihood, not terrain alone, so the terrain roughness and measurement quality are considered. Accordingly, using MI can take into account the errors caused by multimodal distribution that occur in a specific terrain or large measurement errors. Based on the above, I propose an adaptation method using MI. MI is used as an index to judge the measurement quality and the size of the grid support is changed according to the value of the MI. The adaptive algorithm proposed in this dissertation is shown as Fig.3.2. The change in grid size, as shown in Fig.3.2, reduces the size if MI is greater than T, and increases the size if MI is less than T.T is a tuning parameter close to zero. The smaller the T, the more sensitive and the larger the T, the more robust.

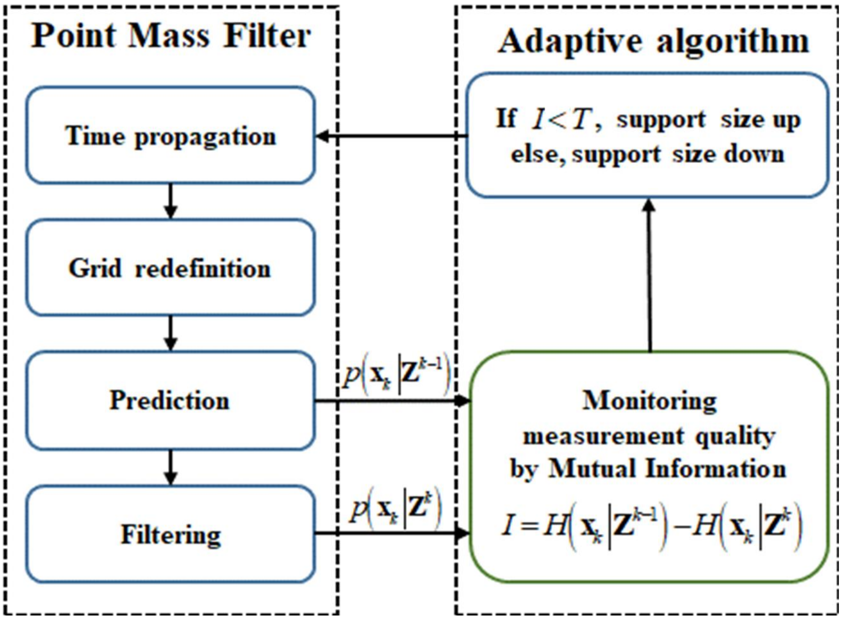

Figure 3.2　Adaptive grid support PMF algorithm

3.2 Numerical Analysis

In this Section, I have performed simulations to verify the performance improvement of the proposed adaptive algorithm. First, the simulation conditions are introduced briefly. Then, I compared the performance of the proposed adaptive grid algorithm with that of the conventional fixed grid. Lastly, the analysis of whether MI was appropriate as an adaptation index has been conducted.

3.2.1 Simulation Conditions

A horizontal resolution of the terrain DB is 3arcsec(≈90m) which is assumed that the length of 1 arcsec is not changed in simulation trajectory, and it is assumed that there is white noise with 5m standard deviation in the database. IMU is assumed by the navigation grade, and it is assumed that barometric altitude and RADAR have only white noise error. Table 3.1 shows parameter specifications.

Table 3.1 IMU and Sensor Specifications

Sensor	Error component	Specification (1-σ)
Accelerometer	Bias	100μg
	Velocity random walk	12μg/rt(Hz)
Gyroscope	Bias	0.01deg/h
	Angular random walk	0.005deg/rt(h)
Barometric altitude	White noise	10m
RADAR	White noise	10m

The velocity is 240m/s in the forward direction and the vertical attitude is set to zero. The initial position error covariance is set equal to the initial position error which is set by 50m(1-σ). The initial grid support of the adaptation algorithm is set at 150m, and the maximum grid support is set at 150m and the minimum at 50m because even if the grid support is larger than 150m, the estimation performance is not affected and in order to maintain robustness, the minimum was set at 50 meters. Simulations are performed on the two trajectories. The first trajectory, Trajectory I, is the area with rough terrain as a whole path and the second trajectory, Trajectory II, is the trajectory over the ocean in the middle of a generally flat area. Fig.3.3 and Fig.3.4 show the terrain elevation map of the Trajectory I and II and change of the terrain elevation under the flight path. The flight paths are set in the north direction along the red line in the figure. 50 Monte Carlo simulations is performed on each trajectory. Results if the graphs are the mean values of Monte Carlo simulations.

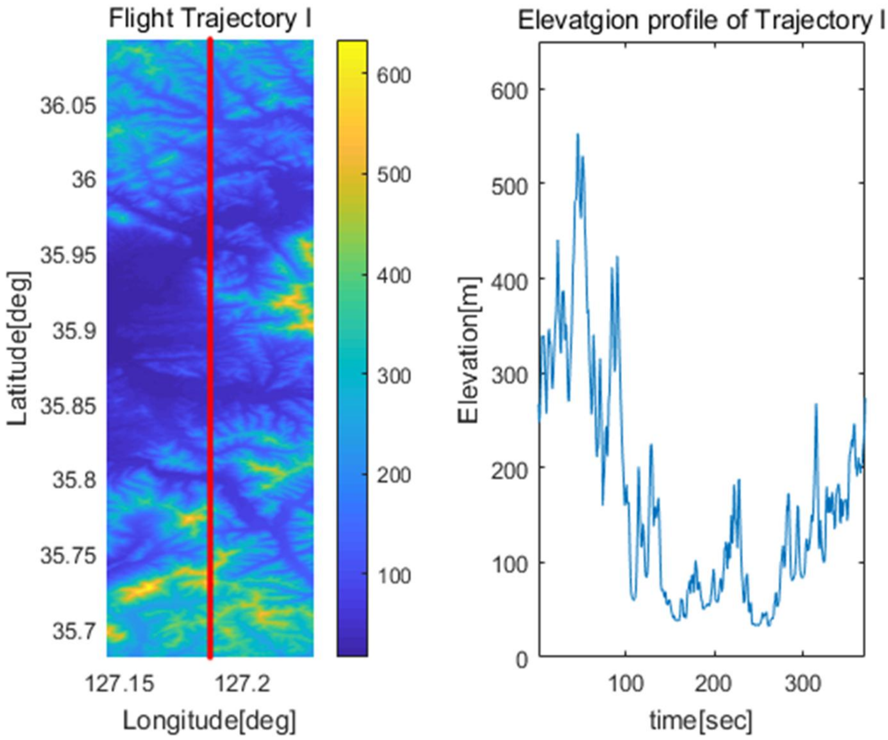

Figure 3.3 Terrain elevation map and elevation profile of Trajectory I

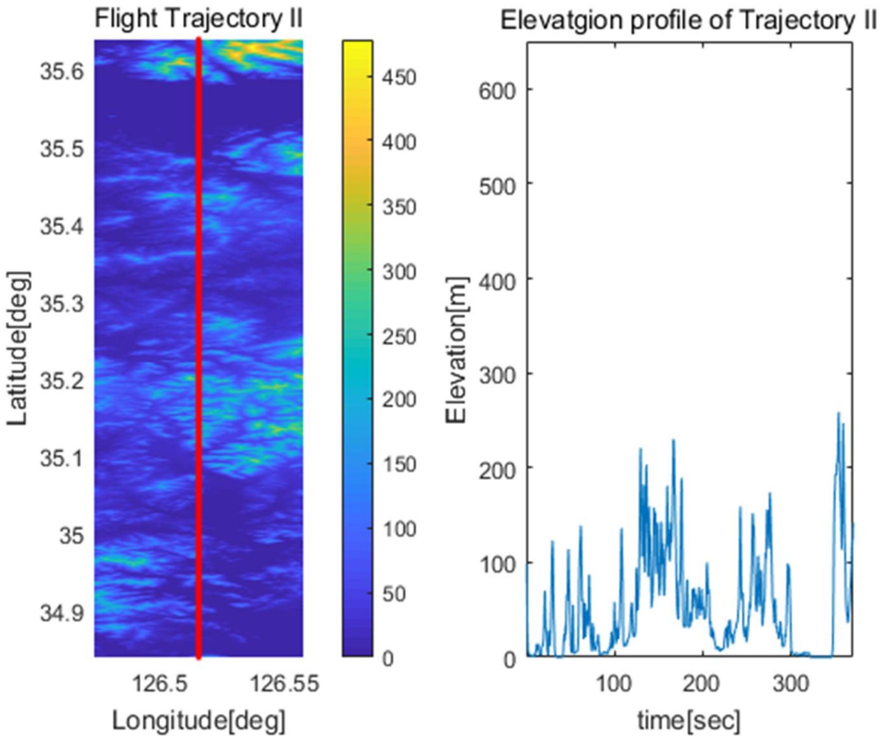

Figure 3.4 Terrain elevation map and elevation profile of Trajectory II

3.2.2 Performance Comparison According to Fixed or Adaptive Grid Support

In order to confirm the performance according to the grid support in the Trajectory I and II, various grid supports are set up and simulations are performed. Grid supports are set at 150m, 100m and 50m. And T of the adaptive parameter is set at 0.05, and the increase and decrease of the grid support size is set to 30m and 10m, respectively because setting a large value has an advantage in an error-increasing section, and setting a small value is advantageous in an error-reducing section. First, the simulation is performed for the Trajectory I. The Trajectory I is generally a path made up of rough areas. The 50 times Monte Carlo simulation results of several grid supports and proposed adaptive method is shown in Fig.3.5, and the change of the grid support is shown in Fig.3.6.

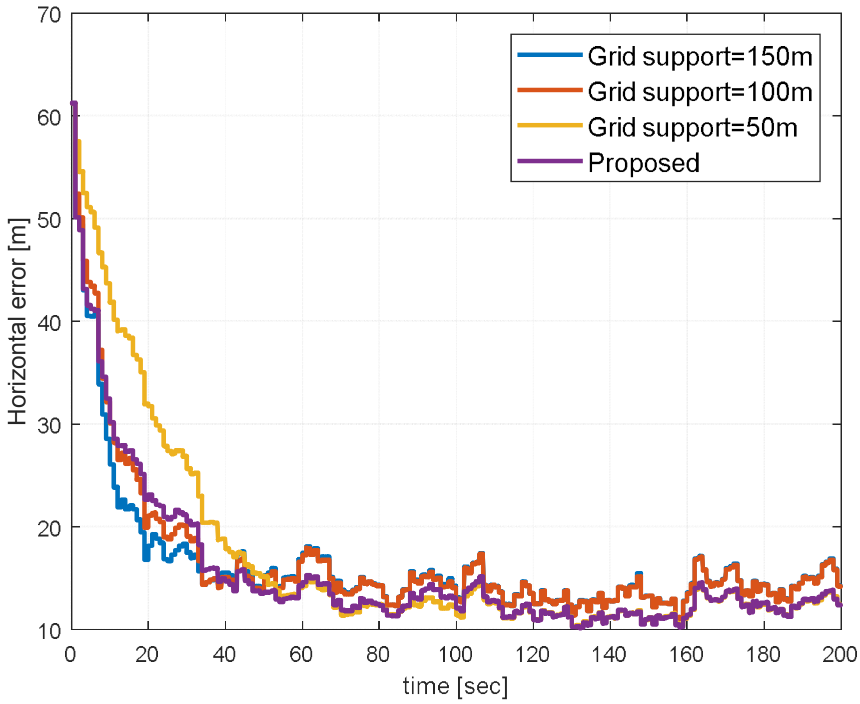

Figure 3.5 Horizontal position errors in Trajectory I

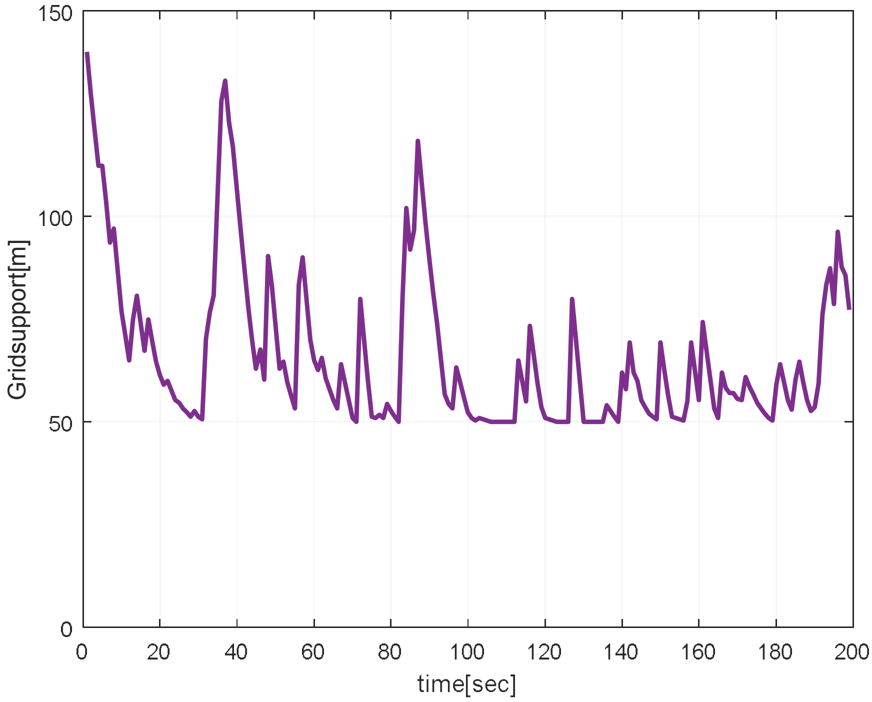

Figure 3.6 Change of the size of the grid support in Trajectory I

Fig.3.5 shows that the larger the grid support size, the faster the convergence speed at the beginning when the error still large. However, if the size of the grid support is small, the convergence speed is low at first, but after the filter converges, the estimation error is smaller than when the grid support is large. Fig.3.6 shows the grid support change of the proposed adaptive algorithm. It can be seen that the flight path is generally rough terrain so that if generally maintains a small grid support. In the case of the adaptive method, the convergence speed is fast and the estimation error after convergence is also kept small. Fig.3.7 and Fig.3.8 show the estimation results and the change of proposed adaptive algorithm for the Trajectory II.

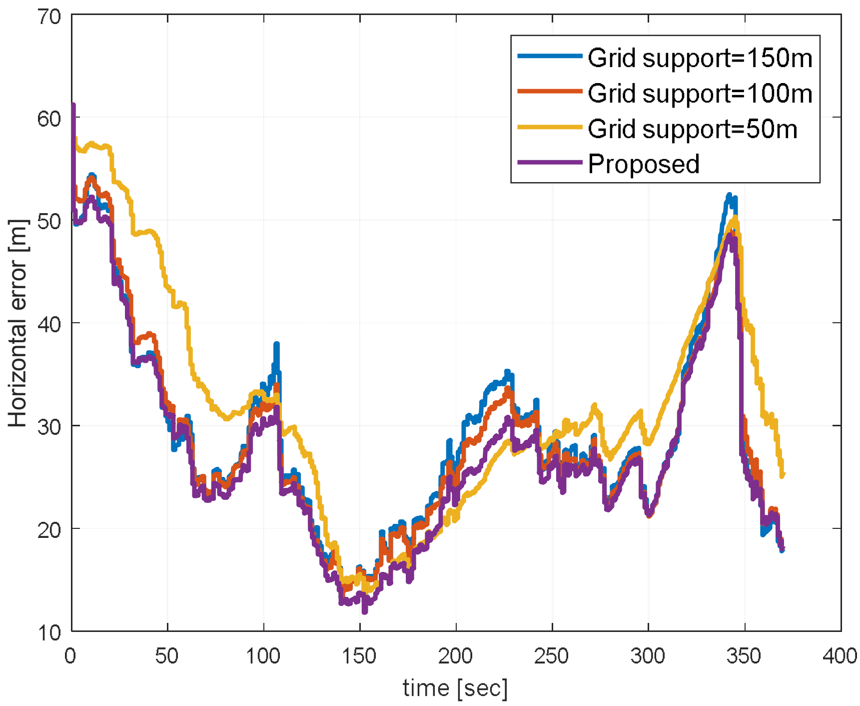

Figure 3.7 Horizontal position errors in Trajectory II

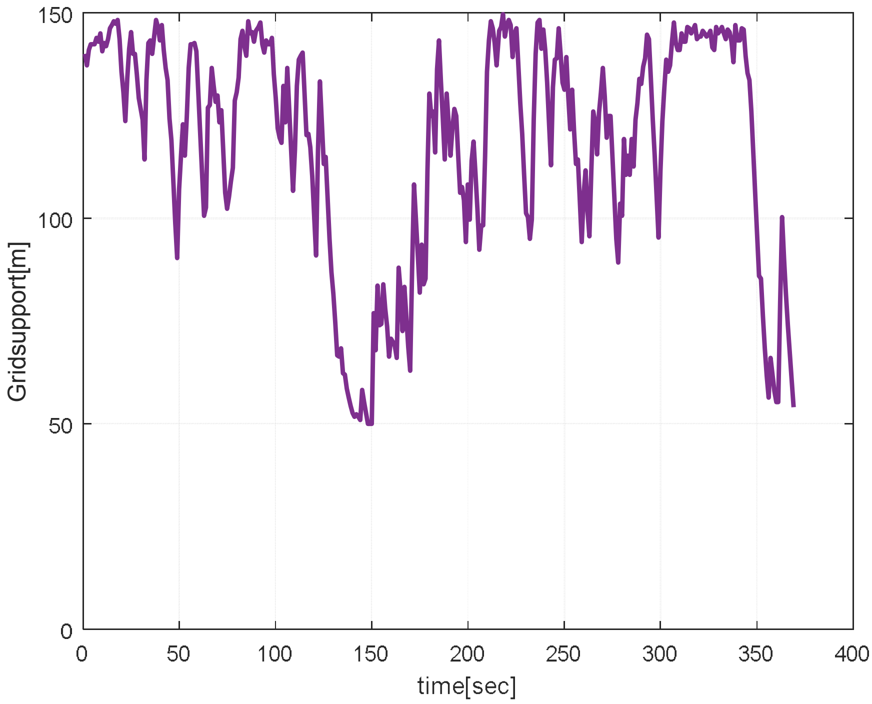

Figure 3.8 Change of the size of the grid support in Trajectory II

The Trajectory II has a generally flat terrain and it is a trajectory passing over the sea in the middle. In the Fig.3.7, it can be seen that the convergence speed is slower in the beginning than the Trajectory I when the grid support is small. Similar to Trajectory I, the estimation performance is better after the filter convergence at 150sec to 200sec, but it diverges more rapidly when the sea is encountered from 300sec to 350sec. In the case of the proposed adaptive method, the estimation performance is good in almost all intervals. In the Fig.3.8, it can be confirmed that the size of the grid support is maintained larger than that in the Trajectory I because most of the terrain is flat. Especially, the grid support is maintained at the maximum size in the interval of 300sec to 350sec passing over the sea. Quantitative results as in Table. 3.3 and 3.4 show that the estimation performance of the proposed algorithm is better than general PMF with fixed grid support. In the computation time of the proposed algorithm which is calculated by tic-toc function in Matlab, it is short in Trajectory I, because the overall small grid is maintained. On the other hand, in the Trajectory II, which is a flat terrain, the grid support is largely maintained and the calculation time is relatively long. Overall, it showed good performance with proposed algorithm and the computation time is also advantageous.

Table 3.2 Quantitative Simulation Results of Trajectory I

Size of grid support	Horizontal RMSE [m]	Computation time [sec]
50m	16.65	38.18
100m	16.33	38.96
150m	15.98	56.26

Adaptation (proposed)	15.14	41.95

Table 3.3 Quantitative Simulation Results of Trajectory II

Size of grid support	Horizontal RMSE [m]	Computation time [sec]
50m	26.30	48.89
100m	24.34	55.84
150m	24.84	80.62
Adaptation (proposed)	23.38	61.53

3.2.3 Analysis of Mutual Information for Adaptive Index

In this Section, I try to analyze whether MI is appropriate as an adaptive index. In the previous section, changes of the grid support seemed to be dominantly influenced by the roughness of the terrain. In other words, the MI value seemed to have a small value when the terrain was flat and a large value when the terrain was rough. Fig.8 shows the change in terrain elevation and MI values over time in trajectory II. Likewise, in this figure, we can see that the change of MI value and the change of terrain elevation are very similar. The roughness of the terrain is calculated as

$$\sigma_T = \sqrt{\frac{1}{n}\sum_{i=1}^{n}\left(H_i - \bar{H}\right)^2} \tag{3.6}$$

where n is the number of the sample, H_i is a height of the i-th grid point and $\bar{H}$ is a mean of the heights [35]. Fig.3.9 shows the relation between MI value and terrain roughness. Also, it shows that the flat terrain has small MI and rough terrain has large MI. Based on these facts, it can be seen that the adaptive method using the MI reflects the roughness of the terrain well.

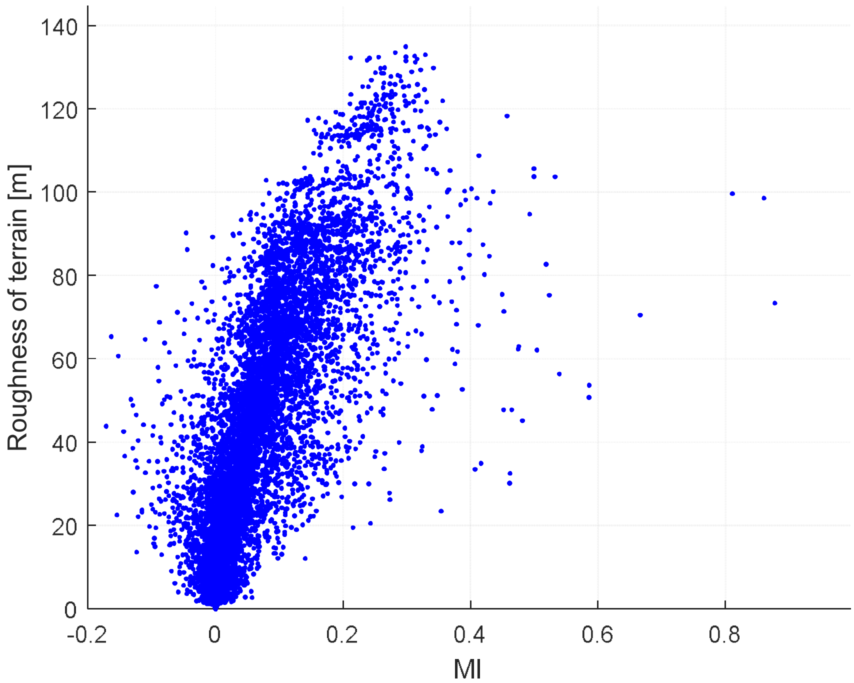

Figure 3.9 Relationship between MI and terrain roughness

But, as shown in the upper left part of Fig.3.9, there is the terrain which is rough but the MI is small. Conversely, in the bottom right part of the figure, the terrain is flat but the MI is large. These parts cannot be considered if the only terrain roughness is used for adaptation method. However, as proposed in this paper, if MI is used as an adaptation index, these exceptions can be considered. Here are examples to support this argument. In the Fig.3.10, the terrain roughness, in left upper part, is 51.8m which can be seen as rough terrain. However, due to the large measurement error, the peak of the likelihood, in the left bottom part, is greatly deviated from the prior estimated position. As a result, although the terrain is sufficiently rough, the estimation error increases as shown in the right two graphs. In this case, MI is smaller than 0, and it means the measurement quality is low despite of rough terrain. Conversely, in the Fig.3.11, the roughness of the terrain is 7.0m which can be seen as flat terrain, but the measurement error is relatively small, and the peak of likelihood don't deviate greatly. So, it can be confirmed that the estimation error is slightly reduced as right two graphs. In this case, MI is larger than 0, and it means the measurement quality is high despite of flat terrain. Based on these examples, MI can be used as an index of adaptation algorithm because it can consider other factors in addition to the terrain roughness.

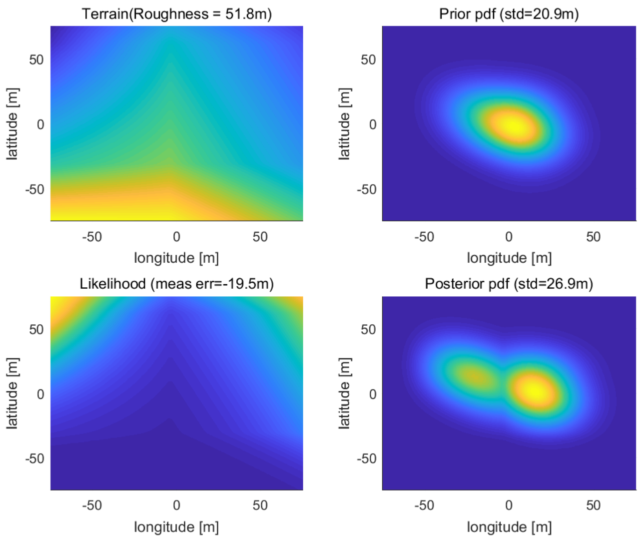

Figure 3.10 Low measurement quality case in the rough terrain with MI < 0

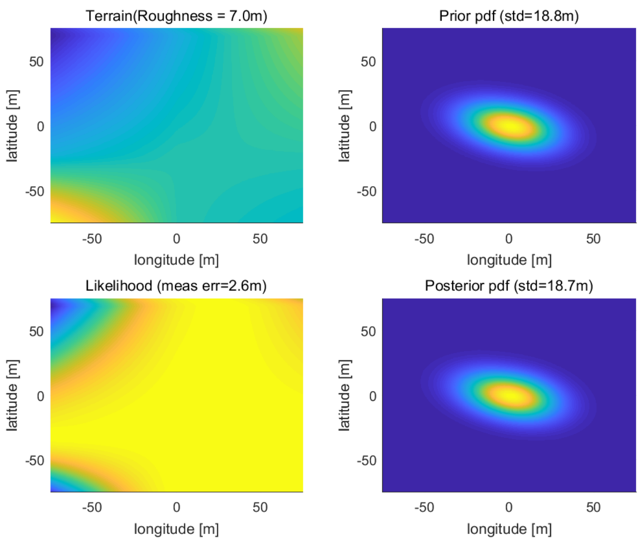

Figure 3.11 High measurement quality case in the flat terrain with MI > 0

3.2.3.1 Comparison Terrain Roughness and MI for Discriminator About Measurement Quality

As shown in figure. 3.9, the terrain roughness and MI are shown by almost linear relationship. So, it might be wondering what is the performance difference when using roughness or MI as an adaptation index. In order to analyze this, it is compared the accuracy of the correction with the case of MI by setting the threshold value to the roughness.

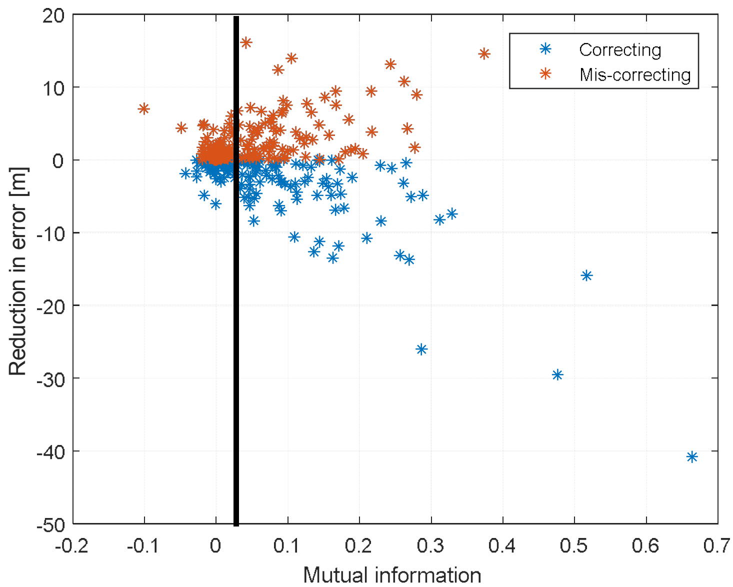

Figure 3.12 The relationship of MI and Reduction in Error

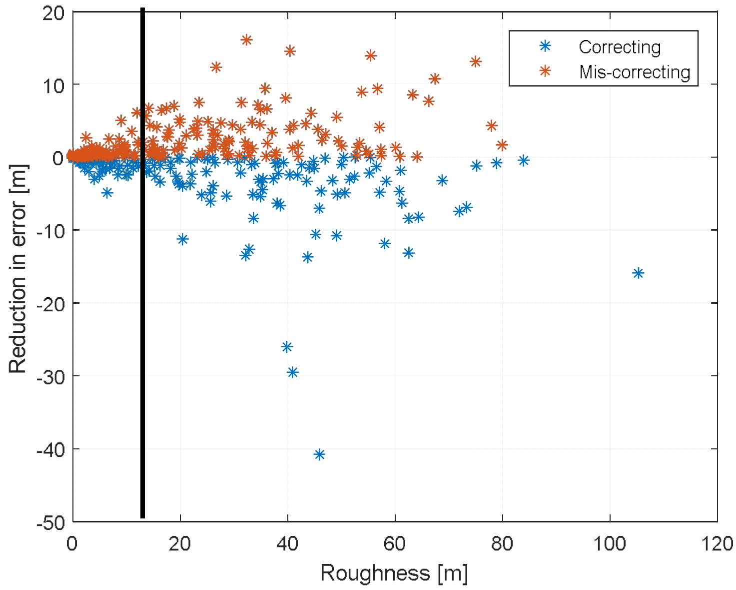

Figure 3.13 The relationship of roughness and Reduction in Error

Figure 3.12 shows the relationship of MI and reduction in error which means the amount of correction due to measurement update and figure 3.13 shows that of roughness for trajectory II. The red dots which are the reduction in error are positive values means that there have been mis-corrected by measurement update, and the blue dot means the opposite. The black lines in figures are threshold and each value is 0.01 and 12m. These values are set to filter out the same amount of mis-correction. The total number of total mis-correction is 204, and the total number of filtered correction is 156 and 157, respectively. In this case, the number of correction (blue dots to the right of the black line) to be filtered is 57 and 65, respectively, and the rate of mis-correction is higher in MI. In other words, MI can be more advantageous in discriminating the measurement quality because the mis-correction by measurement update can be more easily filtered out by MI.

3.3 Summary

In this chapter, I propose an adaptive grid support method of PMF for TRN using MI as an adaptation index. General PMF set the size of the grid support constant and applied it to the TRN, but I find that changing the size of the grid support rather than a constant size improve the estimation performance. So, I adopt MI as an adaptation index to dicriminate measurement quality and to determine changes of the size of the grid support, which can consider not only the roughness of the terrain but also other factors affecting estimation performance. In simulation results, in large position errors and trajectory which flight over the sea in the middle, the estimation performance of the proposed algorithm is better than general PMF that size of the grid support is fixed in the whole trajectory. Also, the computation burden caused by applying the proposed algorithm is insignificant.

Chapter 4

Two Stage Point Mass Filter for State Augmentation

Generally, two or three dimensional state variables that are latitude and longitude, or including height are used in PMF based TRN. As the dimension of state variable increases, its computation burden and its complexity exponentially increase so as to be implemented. To overcome this drawback, Rao-Blackwellized PMF (RBPMF), which estimates linear state variables by linear filters, has been studied by separating nonlinear state variables and linear state variables. However, there is a problem that the amount of computation increases exponentially in the time propagation of the linear state variable, and it has only to be solved by a heuristic method. Besides, there is a disadvantage in that a linear filter of the number of grid points must be operated. To improve this, I propose two stage PMF in this chapter.

4.1 Computational Problem for PMF

4.1.1 2 Dimensional Time Propagation

General PMF based TRN use only two or three state variables, including latitude and longitude, or altitude, in the system model. This is because the amount of computation of the PMF increases exponentially as the number of state variables increases. Especially, in the time propagation process of PMF, it is necessary to consider the relation with all points in order to calculate the density for one point. For example, if the total number of points is N, N repetition calculations are performed to calculate the density at one point, and therefore N^N iterations must be performed to calculate the density at all points.

To solve this problem, PMF based TRN usually uses two-dimensional state variables for latitude and longitude, and uses grid points of square placement with constant point spacing. Let's assume that four simple grid points are propagated by the system model as shown in the following figure.

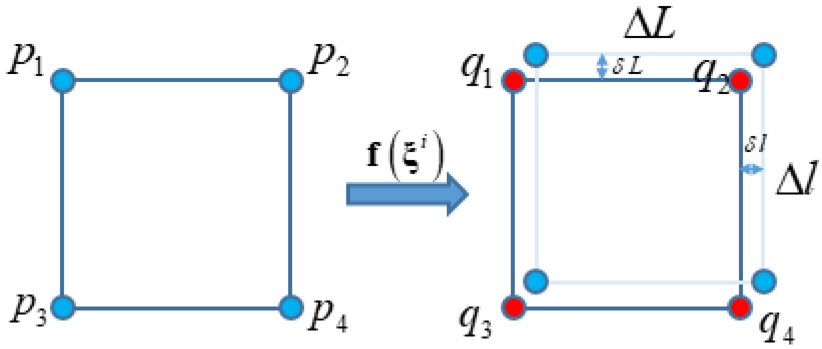

Figure 4.1 Grid point propagation by linear system model for 2 dimension

In TRN, 2 dimensional the system model is a linear model, so each grid point is propagated in parallel by system model as shown in figure 4.1. In the figure, ΔL, Δl are point intervals in the latitudinal and longitudinal directions. The blue points on the left are propagated by δL and δl as shown on the right, and the redesigned points are red points. At this time, the uncertainty of the system model is an additive white Gaussian, so redesigned grid point of q_1 is as follow

$$\begin{aligned} q_1 &= p_1 N\left(\begin{bmatrix}\delta L\\ \delta l\end{bmatrix},\begin{bmatrix}Q_L & 0\\ 0 & Q_l\end{bmatrix}\right) + p_2 N\left(\begin{bmatrix}\delta L+\Delta L\\ \delta l\end{bmatrix},\begin{bmatrix}Q_L & 0\\ 0 & Q_l\end{bmatrix}\right) \\ &\quad + p_3 N\left(\begin{bmatrix}\delta L\\ \delta l+\Delta l\end{bmatrix},\begin{bmatrix}Q_L & 0\\ 0 & Q_l\end{bmatrix}\right) + p_4 N\left(\begin{bmatrix}\delta L+\Delta L\\ \delta l+\Delta l\end{bmatrix},\begin{bmatrix}Q_L & 0\\ 0 & Q_l\end{bmatrix}\right) \\ &= p_1 N(\delta L, Q_L) N(\delta l, Q_l) + p_2 N(\delta L+\Delta L, Q_L) N(\delta l, Q_l) \\ &\quad + p_3 N(\delta L, Q_L) N(\delta l+\Delta l, Q_l) + p_4 N(\delta L+\Delta L, Q_L) N(\delta l+\Delta l, Q_l) \end{aligned} \quad . \tag{4.1}$$

Equation (4.1) can be rewritten as

$$q_1 = \begin{bmatrix} N(\delta L, Q_L) & N(\delta L + \Delta L, Q_L) \end{bmatrix} \begin{bmatrix} p_1 & p_2 \\ p_3 & p_4 \end{bmatrix} \begin{bmatrix} N(\delta l, Q_l) \\ N(\delta l + \Delta l, Q_l) \end{bmatrix}. \tag{4.2}$$

As shown in (4.2), it can be expressed as a matrix multiplication without performing iterative computation. q_1, q_2, q_3 and q_4 can be calculated simultaneously by stacking matrices. For this reason, the amount of computation can be drastically reduced, so only two state variables are used.

4.1.2 3 Dimensional Time Propagation

As described in the previous session, time propagation can be performed without iterative calculation with a simple matrix multiplication for two dimensional state variables. However, it cannot be expressed as a matrix multiplication for state variables for three or more dimensional state variables. Let's assume a 3D grid point as shown in the following figure.

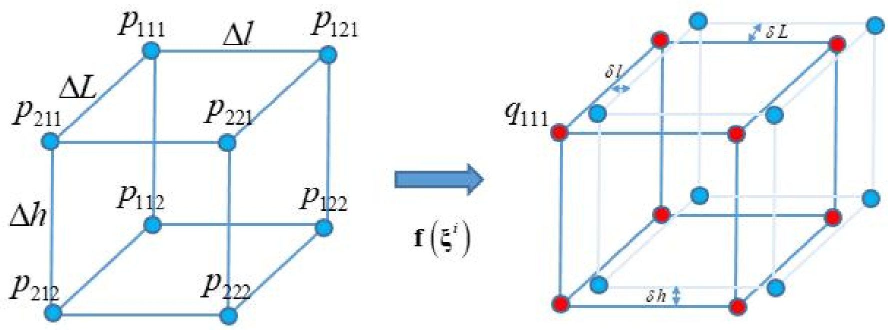

Figure 4.2 Grid point propagation by linear system model for 3 dimension

As in the two dimensions, each point moves in parallel by the linear system model and the probability density for q_{111} is calculated as follows

$$q_{111} = p_{111} N\left(\begin{bmatrix} \delta L \\ \delta l \\ \delta h \end{bmatrix}, \begin{bmatrix} Q_L & 0 & 0 \\ 0 & Q_l & 0 \\ 0 & 0 & Q_h \end{bmatrix} \right) + \cdots + p_{222} N\left(\begin{bmatrix} \delta L + \Delta L \\ \delta l + \Delta l \\ \delta h + \Delta h \end{bmatrix}, \begin{bmatrix} Q_L & 0 & 0 \\ 0 & Q_l & 0 \\ 0 & 0 & Q_h \end{bmatrix} \right) \quad . \quad (4.3)$$

$$= p_{111} N(\delta L, Q_L) N(\delta l, Q_l) N(\delta h, Q_h) + \cdots + p_{222} N(\delta L + \Delta L, Q_L) N(\delta l + \Delta l, Q_l) N(\delta h + \Delta h, Q_h)$$

$$\begin{aligned} &= \left(p_{111} N(\delta L, Q_L) N(\delta l, Q_l) + \cdots + p_{221} N(\delta L + \Delta L, Q_L) N(\delta l + \Delta l, Q_l) \right) N(\delta h, Q_h) \\ &+ \left(p_{112} N(\delta L, Q_L) N(\delta l, Q_l) + \cdots + p_{222} N(\delta L + \Delta L, Q_L) N(\delta l + \Delta l, Q_l) \right) N(\delta h + \Delta h, Q_h) \end{aligned}$$

As (4.2), (4.3) is expressed as a matrix multiplication as follows

$$= \begin{bmatrix} A & B \end{bmatrix} \begin{bmatrix} N(\delta h, Q_h) \\ N(\delta h + \Delta h, Q_h) \end{bmatrix} \quad (4.4)$$

where

$$A = \left[N\left(\delta L, Q_L\right) \quad N\left(\delta L + \Delta L, Q_L\right) \right] \begin{bmatrix} p_{111} & p_{121} \\ p_{211} & p_{221} \end{bmatrix} \begin{bmatrix} N\left(\delta l, Q_l\right) \\ N\left(\delta l + \Delta l, Q_l\right) \end{bmatrix} \quad (4.5)$$

$$B = \left[N\left(\delta L, Q_L\right) \quad N\left(\delta L + \Delta L, Q_L\right) \right] \begin{bmatrix} p_{112} & p_{122} \\ p_{212} & p_{222} \end{bmatrix} \begin{bmatrix} N\left(\delta l, Q_l\right) \\ N\left(\delta l + \Delta l, Q_l\right) \end{bmatrix}. \quad (4.6)$$

As (4.4)-(4.6), 3 matrix multiplications to calculate probability density at one point are needed at two points per dimension. If there are N points per dimension, N matrix multiplications are required to calculate probability density at one point. In other words, if the dimension of the state variables is more than three, time propagation of simple matrix multiplication is not possible as in the two dimension, and the complexity and burden of calculation increases as the state variable increases.

4.2 Rao-Blackwellized Point Mass Filter

In PMF based TRN, the state variable cannot be augmented due to computational burden as mentioned by previous section. Therefore, when the barometric altimeter is not used, the altitude error diverges and the estimation performance deteriorates. Also, since the velocity is not estimated, the position error increases over the time. RBPMF improves the above problem by separating the state variables into nonlinear state variables and linear state variables, estimating nonlinear state variables as PMF, and estimating linear state variables as linear filters. In this section, briefly describe the derivation process of the RBPMF and discuss its problems.

4.2.1 Derivation of Rao-Blackwellized Point Mass Filter

The PMF has robustness to large initial error and nonlinearity of system and measurement equation and it gives global optimal estimate solution. Despite these advantages, there is a drawback that the computation burden increases exponentially as the dimension of the state variable increases. The Rao-Blackwellization (RB) method which is a marginalization technique is the effective approach of reducing the computation burden when it is possible to distinguish between linear and nonlinear state variables. Especially for TRN, the system model can be approximated as a linear system with state variables including position, velocity and attitude, but the measurement model is expressed as a nonlinear function of latitude and longitude. Therefore, latitude and longitude can be set as nonlinear state variables, and altitude, velocity or attitude can be set as linear state variables.

The basic concept of the RB is to separate the state vector as

$$\mathbf{x}_k = \begin{bmatrix} \mathbf{x}_k^n \\ \mathbf{x}_k^l \end{bmatrix} \tag{4.6}$$

where $\mathbf{x}_k^n$ is the nonlinear state variable and $\mathbf{x}_k^l$ is the state variable with conditionally linear. In general case, the system and measurement model become as

$$\mathbf{x}_{k+1}^n = \mathbf{f}_k^n\left(\mathbf{x}_k^n\right) + \mathbf{F}_k^{nl}\mathbf{x}_k^l + \mathbf{w}_k^n \tag{4.7}$$

$$\mathbf{x}_{k+1}^l = \mathbf{f}_k^{ln}\left(\mathbf{x}_k^n\right) + \mathbf{F}_k^l\mathbf{x}_k^l + \mathbf{w}_k^l \tag{4.8}$$

$$\mathbf{z}_k = \mathbf{g}_k^n\left(\mathbf{x}_k^n\right) + \mathbf{G}_k^l\mathbf{x}_k^l + \mathbf{v}_k\,. \tag{4.9}$$

According to the Rao-Blackwellization method, the posterior pdf (2.29) becomes as follows.

$$
\begin{aligned}
p\left(\mathbf{x}_k^j \mid \mathbf{Z}_k\right) \propto p\left(\mathbf{z}_k \mid \mathbf{x}_k^j\right) p\left(\mathbf{x}_k^j \mid \mathbf{Z}_{k-1}\right) \\
= p\left(\mathbf{z}_k \mid \mathbf{x}_k^{n,j}, \mathbf{x}_k^l\right) p\left(\mathbf{x}_k^{n,j}, \mathbf{x}_k^l \mid \mathbf{Z}_{k-1}\right) \\
= p\left(\mathbf{z}_k \mid \mathbf{x}_k^j\right) p\left(\mathbf{x}_k^{n,j} \mid \mathbf{Z}_{k-1}\right) p\left(\mathbf{x}_k^l \mid \mathbf{x}_k^{n,j}, \mathbf{Z}_{k-1}\right)
\end{aligned} \tag{4.10}
$$

where $\mathbf{x}_k^{n,j}$ is j-th nonlinear state variables, $\mathbf{x}_k^{l,j}$ is j-th linear state variables and $p\left(\mathbf{z}_k \mid \mathbf{x}_k^j\right) p\left(\mathbf{x}_k^{n,j} \mid \mathbf{Z}_{k-1}\right)$ can be replaced by the posterior pdf $p\left(\mathbf{x}_k^{n,j} \mid \mathbf{Z}_k\right)$ for nonlinear state variables without considering linear state variables. Then j-th value of the posterior pdf of RBPMF is as follows.

$$
p\left(\mathbf{x}_k^j \mid \mathbf{Z}_k\right) = p\left(\mathbf{x}_k^{n,j} \mid \mathbf{Z}_k\right) p\left(\mathbf{x}_k^l \mid \mathbf{x}_k^{n,j}, \mathbf{Z}_k\right) \tag{4.11}
$$

The pdf of i-th linear state variables $\mathbf{x}_k^{l,j}$ given $\mathbf{x}_k^{n,j}$ and $\mathbf{Z}_{k-1}$ can be written as (4.12) with assumption of the Gaussian pdf, partially linear measurement equation and the Gaussian pdf of the measurement noise.

$$
p\left(\mathbf{x}_k^l \mid \mathbf{x}_k^{n,j}, \mathbf{Z}_{k-1}\right) = N\left(\mathbf{x}_k^l, \hat{\mathbf{x}}_k^{l,j+}, \mathbf{P}_k^{l,j+}\right) \tag{4.12}
$$

where

$$
\begin{aligned}
\hat{\mathbf{x}}_k^{l,j+} &= \hat{\mathbf{x}}_k^{l,j-} + \mathbf{K}_k^j\left(\mathbf{z}_k - \mathbf{h}_k\left(\mathbf{x}_k^{n,j}\right) - \mathbf{H}_k \hat{\mathbf{x}}_k^{l,j-}\right) \\
\mathbf{P}_k^{l,j+} &= \mathbf{P}_k^{l,j-} - \mathbf{K}_k^j \mathbf{H}_k \mathbf{P}_k^{l,j-} \\
\mathbf{K}_k^j &= \mathbf{P}_k^{l,j-} \mathbf{H}_k^T \left(\mathbf{H}_k \mathbf{P}_k^{l,j-} \mathbf{H}_k^T + \mathbf{R}_k\right)^{-1}
\end{aligned} \tag{4.13}
$$

As in (4.12), since each grid point for nonlinear state variables is given, there are N estimates of the linear state variables for each grid point.

Next, the prior pdf becomes as follows

$$
\begin{aligned}
p\left(\mathbf{x}_k^j \mid \mathbf{Z}_{k-1}\right) &= \sum_{i=1}^{N} p\left(\mathbf{x}_k^j \mid \mathbf{x}_{k-1}^i\right) p\left(\mathbf{x}_{k-1}^i \mid \mathbf{Z}_{k-1}\right) \\
&= \sum_{i=1}^{N} p\left(\mathbf{x}_k^{n,j}, \mathbf{x}_k^l \mid \mathbf{x}_{k-1}^{n,i}, \mathbf{x}_{k-1}^l\right) p\left(\mathbf{x}_{k-1}^{n,i}, \mathbf{x}_{k-1}^l \mid \mathbf{Z}_{k-1}\right)
\end{aligned}
\tag{4.14}
$$

where the conditional probability property is used and

$$
p\left(\mathbf{x}_k^{n,j}, \mathbf{x}_k^l \mid \mathbf{x}_{k-1}^{n,i}, \mathbf{x}_{k-1}^l\right) = p\left(\mathbf{x}_k^l \mid \mathbf{x}_k^{n,j}, \mathbf{x}_{k-1}^{n,i}, \mathbf{x}_{k-1}^l\right) p\left(\mathbf{x}_k^{n,j} \mid \mathbf{x}_{k-1}^{n,i}, \mathbf{x}_{k-1}^l\right) \tag{4.15}
$$

$$
p\left(\mathbf{x}_{k-1}^{n,i}, \mathbf{x}_{k-1}^l \mid \mathbf{Z}_{k-1}\right) = p\left(\mathbf{x}_k^l \mid \mathbf{x}_{k-1}^{n,i}, \mathbf{Z}_{k-1}\right) p\left(\mathbf{x}_{k-1}^{n,i} \mid \mathbf{Z}_{k-1}\right). \tag{4.16}
$$

Substituting (4.15) and (4.16) into (4.14) can be rewritten as follows

$$
\begin{aligned}
p\left(\mathbf{x}_k^j \mid \mathbf{Z}_{k-1}\right) &= \sum_{i=1}^{N} p\left(\mathbf{x}_k^{n,j} \mid \mathbf{x}_{k-1}^{n,i}, \mathbf{x}_{k-1}^l\right) p\left(\mathbf{x}_{k-1}^{n,i} \mid \mathbf{Z}_{k-1}\right) \\
&\qquad p\left(\mathbf{x}_k^l \mid \mathbf{x}_k^{n,j}, \mathbf{x}_{k-1}^{n,i}, \mathbf{x}_{k-1}^l\right) p\left(\mathbf{x}_k^l \mid \mathbf{x}_{k-1}^{n,i}, \mathbf{Z}_{k-1}\right) \\
&= \sum_{i=1}^{N} p\left(\mathbf{x}_k^{n,j} \mid \mathbf{x}_{k-1}^{n,i}, \mathbf{x}_{k-1}^l\right) p\left(\mathbf{x}_{k-1}^{n,i} \mid \mathbf{Z}_{k-1}\right) \\
&\qquad p\left(\mathbf{x}_k^l \mid \mathbf{x}_k^{n,j}, \mathbf{x}_{k-1}^{n,i}, \mathbf{x}_{k-1}^l, \mathbf{Z}_{k-1}\right) \\
&= \sum_{i=1}^{N} p\left(\mathbf{x}_k^{n,j} \mid \mathbf{x}_{k-1}^{n,i}, \mathbf{x}_{k-1}^l\right) p\left(\mathbf{x}_{k-1}^{n,i} \mid \mathbf{Z}_{k-1}\right) \\
&\qquad p\left(\mathbf{x}_k^l \mid \mathbf{x}_k^{n,j}, \mathbf{x}_{k-1}^{n,i}, \mathbf{Z}_{k-1}\right) p\left(\mathbf{x}_k^l \mid \mathbf{x}_{k-1}^{n,i}, \mathbf{x}_{k-1}^l\right)
\end{aligned}
\tag{4.17}
$$

where $\sum_{i=1}^{N} p\left(\mathbf{x}_k^{n,j} \mid \mathbf{x}_{k-1}^{n,i}, \mathbf{x}_{k-1}^{l}\right) p\left(\mathbf{x}_{k-1}^{n,i} \mid \mathbf{Z}_{k-1}\right)$ can be replaced by the prior pdf $p\left(\mathbf{x}_k^{n,j} \mid \mathbf{Z}_{k-1}\right)$ which not consider linear state variables. As shown in (4.11), (4.17) can also be expressed as pdf for the nonlinear state variables with pdf for the linear state variables as follows

$$p\left(\mathbf{x}_k^{j} \mid \mathbf{Z}_{k-1}\right) = p\left(\mathbf{x}_k^{n,j} \mid \mathbf{Z}_{k-1}\right) \sum_{i=1}^{N} p\left(\mathbf{x}_k^{l} \mid \mathbf{x}_k^{n,j}, \mathbf{x}_{k-1}^{n,i}, \mathbf{Z}_{k-1}\right) p\left(\mathbf{x}_k^{l} \mid \mathbf{x}_{k-1}^{n,i}, \mathbf{x}_{k-1}^{l}\right). \tag{4.17}$$

The term in the sigma of (4.17) which is the pdf of the time propagation can be written as (4.18) with assumption of the Gaussian pdf

$$\sum_{i=1}^{N} p\left(\mathbf{x}_k^{l} \mid \mathbf{x}_k^{n,j}, \mathbf{x}_{k-1}^{n,i}, \mathbf{Z}_{k-1}\right) p\left(\mathbf{x}_k^{l} \mid \mathbf{x}_{k-1}^{n,i}, \mathbf{x}_{k-1}^{l}\right) = \sum_{i=1}^{N} N\left(\mathbf{x}_k^{l}; \hat{\mathbf{x}}_k^{l,(i,j)-}, \mathbf{P}_k^{l,(i,j)-}\right). \tag{4.18}$$

where

$$\hat{\mathbf{x}}_k^{l,(i,j)-} = \mathbf{f}_{k-1}^{ln}\left(\mathbf{x}_{k-1}^{n,i}\right) + \mathbf{F}_{k-1}^{l} \hat{\mathbf{x}}_{k-1}^{l,(i,j)+} \tag{4.19}$$

$$\mathbf{P}_k^{l,(i,j)-} = \mathbf{F}_{k-1}^{l} \mathbf{P}_{k-1}^{l,(i,j)+} \left(\mathbf{F}_{k-1}^{l}\right)^T + \mathbf{Q}_k^{l} \tag{4.20}$$

$$\hat{\mathbf{x}}_{k-1}^{l,(i,j)+} = \hat{\mathbf{x}}_{k-1}^{l,i+} + \mathbf{K}_{k-1}^{(i,j)} \left(\mathbf{y}_{k-1}^{(i,j)} - \mathbf{F}_{k-1}^{nl} \hat{\mathbf{x}}_{k-1}^{l,i+}\right) \tag{4.21}$$

$$\mathbf{P}_{k-1}^{l,(i,j)+} = \mathbf{P}_{k-1}^{l,i} - \mathbf{K}_{k-1}^{(i,j)} \mathbf{F}_{k-1}^{nl} \mathbf{P}_{k-1}^{l,i} \tag{4.22}$$

$$\mathbf{K}_{k-1}^{(i,j)} = \mathbf{P}_{k-1}^{l,i} \left(\mathbf{F}_k^{nl}\right)^T \left(\mathbf{F}_{k-1}^{nl} \mathbf{P}_{k-1}^{l,i} \left(\mathbf{F}_{k-1}^{nl}\right)^T + \mathbf{Q}_k^{n}\right)^{-1} \tag{4.23}$$

$$\mathbf{y}_{k-1}^{(i,j)} = \mathbf{x}_k^{n,j} - \mathbf{f}_{k-1}^{n}\left(\mathbf{x}_{k-1}^{n,i}\right) \tag{4.24}$$

4.2.2 Problem in Rao-Blackwellized Point Mass Filter

The above equation has a structure similar to a general Kalman filter. Equation (4.21) and (4.22) are equivalent to the measurement update using the artificial measurement (4.24), and (4.19) and (4.20) are equivalent to time propagation using the system model. By the way, there is a big problem that heavy computation is needed in this process. This is because, in order to estimate the linear state variable at the jth point at time k, the relation with all the points at time k-1 must be considered to artificial measurement, as in (4.24). For this reason, in jth point at time k, estimates are calculated as the number of the grid points at time k-1 and the problem of how to merge them also occurs. Authors in [72] solved this problem through moment matching and heuristic technique, but the optimal solution has not yet been studied.

4.3 Two Stage Point Mass Filter

The two stage filtering is a way to operate two filters in parallel by separating the dynamic state variable and the bias state variables [73-78]. The two filters are a bias free filter which estimate the dynamic state variables and a bias filter for estimating bias state variables respectively and correction is performed taking into consideration the correlation between each other. In many researches, few studies have applied different filters to these two filters. There are studies using the name “two stage” but did not succeed to the concept of the previous studies. We inherited the original two stage method and approach to benefit from applying different filters to the two filters. The main concept of the proposed algorithm is that, in PMF based TRN, the latitude and longitude that cause large nonlinearity in the measurement model are estimated by PMF, and the altitude or including velocity are estimated by using linear filter. This can greatly reduce the amount of computation and simplify the configuration, even if the state variable is further augmented rather than RBPMF.

4.3.1 Two Stage Filtering

Consider the linear stochastic system and measurement model as follows

$$\mathbf{d}_{k+1} = \mathbf{A}_k \mathbf{d}_k + \mathbf{B}_k \mathbf{b}_k + \mathbf{w}_k^d \tag{4.25}$$

$$\mathbf{b}_{k+1} = \mathbf{D}_k \mathbf{b}_k + \mathbf{w}_k^b \tag{4.26}$$

$$\mathbf{z}_k = \mathbf{H}_{d,k}\mathbf{d}_k + \mathbf{H}_{b,k}\mathbf{b}_k + \mathbf{v}_k \tag{4.27}$$

where $\mathbf{d}_k$ is the dynamic state vector, $\mathbf{b}_k$ is the bias state vector and $\mathbf{z}_k$ is the measurement vector. $\mathbf{A}_k$, $\mathbf{B}_k$, $\mathbf{D}_k$, $\mathbf{H}_{d,k}$,and $\mathbf{H}_{b,k}$ are matrices of dynamic, bias and measurement, respectively. $\mathbf{w}_k^d$, $\mathbf{w}_k^b$ and $\mathbf{v}_k$ are zero mean uncorrelated Gaussian random noise of system, bias and measurement model and its covariance are $\mathbf{Q}_k^d$, $\mathbf{Q}_k^b$, and $\mathbf{R}_k$.

The two stage filter is given by the following equations when the stochastic system and measurement model given as (4.25) - (4.27)

$$\hat{\mathbf{d}}_k^- = \overline{\mathbf{d}}_k^- + \mathbf{U}_k \overline{\mathbf{b}}_k^- \tag{4.28}$$

$$\hat{\mathbf{d}}_k^+ = \overline{\mathbf{d}}_k^+ + \mathbf{V}_k \overline{\mathbf{b}}_k^- \tag{4.29}$$

$$\mathbf{P}_k^{d-} = \overline{\mathbf{P}}_k^{d-} + \mathbf{U}_k \overline{\mathbf{P}}_k^{b-} \mathbf{U}_k^T \tag{4.30}$$

$$\mathbf{P}_k^{d+} = \overline{\mathbf{P}}_k^{d+} + \mathbf{V}_k \overline{\mathbf{P}}_k^{b+} \mathbf{V}_k^T \tag{4.31}$$

where $\hat{\mathbf{d}}_k^{(\cdot)}$ is the estimate of the dynamic state variables and $\mathbf{P}_k^{d(\cdot)}$ is its covariance matrix with the assumption that the biases are perfectly known. $\overline{\mathbf{d}}_k^{(\cdot)}$ is the estimate of the dynamic state variable with the assumption that there are no biases and its covariance is $\bar{\mathbf{P}}_k^{d(\cdot)}$. $\bar{\mathbf{b}}_k^{(\cdot)}$, and $\bar{\mathbf{P}}_k^{b(\cdot)}$ are the estimate of the bias state variable and covariance. $\mathbf{U}_k$, and $\mathbf{V}_k$ are sensitivity matrices to be defined. The variables with (-) superscript mean a prior estimate and covariance and the variables with (+) superscript mean a posterior estimate and covariance. The two stage filter is decomposed into the bias free filter and bias filter. The bias free filter gives $\bar{\mathbf{d}}_k^{(\cdot)}$, and $\bar{\mathbf{P}}_k^{d(\cdot)}$, and the bias filter gives $\bar{\mathbf{b}}_k^{(\cdot)}$ and $\bar{\mathbf{P}}_k^{b(\cdot)}$. After estimating in each filter, the corrected estimate $\hat{\mathbf{d}}_k^{(\cdot)}$ and covariance $\mathbf{P}_k^{d(\cdot)}$ is obtained from each estimate of the two filters and coupling equations as in (4.28) - (4.31). The bias free filter is as follows

$$\bar{\mathbf{d}}_k^- = \mathbf{A}_{k-1}\bar{\mathbf{x}}_{k-1}^+ \tag{4.32}$$

$$\bar{\mathbf{P}}_k^{d-} = \mathbf{A}_{k-1}\bar{\mathbf{P}}_{k-1}^{d+}\mathbf{A}_{k-1}^T + \mathbf{Q}_{k-1}^d \tag{4.33}$$

$$\mathbf{K}_k^d = \bar{\mathbf{P}}_k^{d-}\mathbf{H}_{d,k}^T\left(\mathbf{H}_{d,k}\bar{\mathbf{P}}_k^{d-}\mathbf{H}_{d,k}^T + \mathbf{R}_k\right)^{-1} \tag{4.34}$$

$$\bar{\mathbf{P}}_k^{d+} = \left(\mathbf{I} - \mathbf{K}_k^d\mathbf{H}_{d,k}\right)\bar{\mathbf{P}}_k^{d-} \tag{4.35}$$

$$\bar{\mathbf{d}}_k^+ = \bar{\mathbf{d}}_k^- + \mathbf{K}_k^d\left(\mathbf{z}_k - \mathbf{H}_{d,k}\bar{\mathbf{d}}_k^-\right) \tag{4.36}$$

where $\mathbf{K}_k^d$ is a Kalman gain for bias free filter to estimate dynamic state variables. The bias filter is as follows

$$\bar{\mathbf{b}}_k^- = \mathbf{D}_{k-1}\bar{\mathbf{b}}_{k-1}^+ \tag{4.37}$$

$$\bar{\mathbf{P}}_k^{b-} = \mathbf{D}_{k-1}\bar{\mathbf{P}}_{k-1}^{b+}\mathbf{D}_{k-1}^T + \mathbf{Q}_{k-1}^b \tag{4.38}$$

$$\mathbf{K}_k^b = \overline{\mathbf{P}}_k^{b-}\mathbf{S}_k^T\left(\mathbf{H}_{1,k}\overline{\mathbf{P}}_k^{d-}\mathbf{H}_{1,k}^T + \mathbf{S}_k\overline{\mathbf{P}}_k^{b-}\mathbf{S}_k^T + \mathbf{R}_k\right)^{-1} \tag{4.39}$$

$$\overline{\mathbf{P}}_k^{b+} = \left(\mathbf{I} - \mathbf{K}_k^b\mathbf{S}_k\right)\overline{\mathbf{P}}_k^{b-} \tag{4.40}$$

$$\overline{\mathbf{b}}_k^+ = \overline{\mathbf{b}}_k^- + \mathbf{K}_k^b\left(\mathbf{z}_k - \mathbf{S}_k\overline{\mathbf{d}}_k^- - \mathbf{H}_{b,k}\overline{\mathbf{b}}_k^-\right) \tag{4.41}$$

where $\mathbf{K}_k^b$ is a Kalman gain for bias filter to estimate bias state variables and k-th the coupling equations

$$\mathbf{S}_k = \mathbf{H}_{d,k}\mathbf{U}_k + \mathbf{H}_{b,k} \tag{4.42}$$

$$\mathbf{U}_k = \left(\mathbf{A}_{k-1}\mathbf{V}_{k-1} + \mathbf{B}_{k-1}\right)\mathbf{D}_k^{-1} \tag{4.43}$$

$$\mathbf{V}_k = \mathbf{U}_k - \mathbf{K}_k^d\mathbf{S}_k \tag{4.44}$$

where $\mathbf{S}_k$, $\mathbf{U}_k$ and $\mathbf{V}_k$ are called sensitivity matrices and its derivation process are summarized in [75].

As described above, it can be separated into two parallel filter for bias free filter and bias filter. The original purpose of two stage filter is to avoid hard computational effort due to augment bias state to state variables. However, even if they are not dynamic state variables and bias state variables, there is no problem to apply two stage filter if the system model configuration is same as (4.25) - (4.27). Because $\mathbf{F}_k^{ln}$ is zero, the system and measurement model for TRN have same configuration with (4.25) - (4.27) (see, Section 4.3.3), so it can be applied to two stage filter. Even if the velocity or attitude is included in the state variables, since

$\mathbf{F}_k^{ln}$ is zero, so there is no problem to apply two stage filter.

4.3.2 Two Stage Point Mass Filter Algorithm

In PMF based TRN, because of the computation burden in time propagation as in (2.30), only latitude and longitude are set as state variables, or including height. Although applying RBPMF for augmenting state variables, the problem of the amount of computation still exists due to the iterative operation of (4.19) - (4.24). To solve this problem, we describe the proposed algorithm which is called by two stage point mass filter (TSPMF) in this section. The main idea of the TSPMF is to apply the two stage filtering to augment the state variable in the PMF based TRN. In first stage, the bias free filter of (4.32) - (4.36) in two stage filter replaces the general PMF based TRN estimating nonlinear states which are latitude and longitude. In second stage, $\mathbf{K}_k^n$, and $\mathbf{H}_{n,k}$, corresponding $\mathbf{K}_k^d$, and $\mathbf{H}_{d,k}$ in bias free filter, should be calculated first for estimating linear state which is altitude. But they do not exist because PMF is applied in the first stage. But it can be obtained by analytically because PMF applied in first stage doesn't have matrix form of Kalman gain and measurement matrix. So, it should be calculated numerically. $\mathbf{H}_{d,k}$ can be obtained easily by numerically differentiating $\mathbf{g}_k(\cdot)$ and its process is described in [64] . To calculate $\mathbf{K}_k^d$, the moment matching technique can be adopted as follows

$$\mathbf{S}_k = \sum_j \left(\mathbf{g}_k\left(\mathbf{x}_k^{n,j}\right) - \mu_k\right)\left(\mathbf{g}_k\left(\mathbf{x}_k^{n,j}\right) - \mu_k\right)^T p\left(\mathbf{x}_k^{n,j} \mid \mathbf{Z}_{k-1}\right) \tag{4.45}$$

$$\mathbf{C}_k = \sum_j \left(\mathbf{x}_k^{n,j} - \mathbf{x}_k^{n-}\right)\left(\mathbf{g}_k\left(\mathbf{x}_k^{n,j}\right) - \mu_k\right)^T p\left(\mathbf{x}_k^{n,j} \mid \mathbf{Z}_{k-1}\right) \tag{4.46}$$

$$\mathbf{K}_k^n = \mathbf{C}_k \mathbf{S}_k^{-1} \tag{4.47}$$

where

$$\mu_k = \sum_j \mathbf{g}_k\left(\mathbf{x}_k^{n,j}\right) p\left(\mathbf{x}_k^{n,j} \mid \mathbf{Z}_{k-1}\right) \tag{4.48}$$

$$\mathbf{x}_k^{n-} = \sum_j \mathbf{x}_k^{n,j} p\left(\mathbf{x}_k^{n,j} \mid \mathbf{Z}_{k-1}\right) \tag{4.49}$$

where $\mathbf{S}_k$ is an estimated innovation covariance, $\mathbf{C}_k$ is a estimated correlated covariance, $\mathbf{K}_k^n$ is an estimated Kalman gain for first stage filter, μ_k is an estimated measurement which is a sample mean of measurement function and $\mathbf{x}_k^{n-}$ is a sample mean of the prior pdf.

Finally, the bias filter corresponding to (4.37) - (4.41) applies the EKF for estimating the altitude by using $\mathbf{K}_k^n$ and $\mathbf{H}_{d,k}$ in second stage. This method has the disadvantage of damaging optimality by using moment matching. However, since only one filter is used to estimate the linear state variable, the amount of computation can be greatly reduced compared to the general PMF or RBPMF with extended state variables. Problems arising from numerical differentiation of measurement matrices and problems caused by moment matching are discussed in sub-session 4.4.2.1 and 4.4.2.2.The overall TSPMF algorithm is as in Table.4.1 and system and measurement models are defined by sub-section 4.3.3

Table 4.1 TSPMF algorithm

Initialize Set $p\left(\mathbf{x}_0^n \middle| \mathbf{Z}_0\right)$, $\mathbf{P}_0^{l+}$, $\mathbf{x}_0^n$ and $\mathbf{x}_0^n$ **First stage** - Estimate nonlinear states by PMF $\mathbf{x}_k^{n,j} = \left[L_k \quad l_k\right]^T$ **(** L_k : latitude, l_k : longitude) $p\left(\mathbf{x}_k^{n,j} \mid \mathbf{Z}_{k-1}\right) = \sum_{i=1}^{N} p\left(\mathbf{x}_k^{n,j} \mid \mathbf{x}_{k-1}^{n,i}\right) p\left(\mathbf{x}_{k-1}^{n,i} \mid \mathbf{Z}_{k-1}\right)$ $p\left(\mathbf{x}_k^{n,j} \mid \mathbf{Z}_k\right) \propto p\left(\mathbf{z}_k \mid \mathbf{x}_k^{n,j}\right) p\left(\mathbf{x}_k^{n,j} \mid \mathbf{Z}_{k-1}\right)$ where L_k is latitude and l_k is longitude. **Second stage** - Calculate $\mathbf{H}_{n,k}$, $\mathbf{K}_k^d$ by numerical differentiation and moment matching as (4.45) – (4.49) - Estimate linear state by Kalman filter $x_k^l = h_k$ **(** h_k : height) $\overline{x}_k^- = F_{k-1}^l \overline{x}_{k-1}^+$ $\overline{P}_k^{l-} = F_{k-1}^l \overline{P}_{k-1}^{l+} \left(F_{k-1}^l\right)^T + Q_{k-1}^l$ $K_k^l = \overline{P}_k^{l-} S_k^T \left(H_{l,k} \overline{P}_k^{l-} H_{l,k}^T + S_k \overline{P}_k^{l-} S_k^T + R_k\right)^{-1}$ $\overline{P}_k^{l+} = \left(I - K_k^l S_k\right) \overline{P}_k^{l-}$ $\overline{x}_k^{l+} = \overline{x}_k^{l+} + K_k^b \left(z_k - \mathbf{H}_{n,k} \overline{\mathbf{x}}_k^{n-} - S_k \overline{x}_k^{l-}\right)$ where h_k is height, and sensitivity matrices are $S_k = \mathbf{H}_{n,k} \mathbf{U}_k + H_{l,k}$ $\mathbf{U}_k = \left(\mathbf{F}_{k-1}^n \mathbf{V}_{k-1} + \mathbf{F}_{k-1}^{nl}\right) \left(F_k^l\right)^{-1}$ $\mathbf{V}_k = \mathbf{U}_k - \mathbf{K}_k^n S_k$ - Correct the estimates and covariance as (4.28) – (4.31)

4.3.3 Applying to Terrain Referenced Navigation

In general, for Bayesian filter based TRN, the system model is used by linear model, in which the position of the vehicle is set as state variables as follows

$$\mathbf{x}_{k+1} = \mathbf{F}_k \mathbf{x}_k + \mathbf{T}_k \mathbf{u}_k + \mathbf{w}_k \tag{4.50}$$

$$\mathbf{F}_k = \mathbf{I}_{3\times3}, \qquad \mathbf{T}_k = diag\begin{bmatrix} 1/R_e & 1/R_e & -1 \end{bmatrix} \tag{4.51}$$

$$\mathbf{x}_k = \begin{bmatrix} L_k & l_k & h_k \end{bmatrix}^T, \qquad \mathbf{u}_k = \begin{bmatrix} V_N & V_E & V_D \end{bmatrix}^T \tag{4.52}$$

where $\mathbf{F}_k$ is a system matrix, $\mathbf{T}_k$ is a input matrix, R_e is earth radius, L_k, l_k, and h_k are latitude, longitude and height, the input vector $\mathbf{u}_k$ which contain V_N, V_E, and V_D is velocity for the navigation frame of north, east and down axis. RADAR altimeter which measure a range between the ground and the vehicle is used for TRN and measurement model as in (2.34) becomes as follows

$$z_k = \mathbf{g}_k(\mathbf{x}_k) + v_k \tag{4.53}$$

$$\mathbf{g}_k(\mathbf{x}_k) = -h_k^{DB}(L_k, l_k) + h_k \tag{4.54}$$

where $h_k^{DB}(\cdot)$ is the terrain elevation obtained by DEM and h_k is altitude of the vehicle. The pdf $p(\mathbf{w}_k)$, and $p(v_k)$ are assumed to be Gaussian distribution.

To apply for RBPMF based TRN, the state variables are separated nonlinear and linear as

$$\mathbf{x}_k^n = \begin{bmatrix} L_k \\ l_k \end{bmatrix},\ x_k^l = h_k \tag{4.55}$$

and the system and measurement model also should be divided as

$$\mathbf{F}_k = \begin{bmatrix} \mathbf{F}_k^n & \mathbf{F}_k^{nl} \\ \mathbf{F}_k^{ln} & \mathbf{F}_k^l \end{bmatrix} \tag{4.56}$$

$$\mathbf{g}_k\left(\mathbf{x}_k\right) = \mathbf{g}_k^n\left(\mathbf{x}_k^n\right) + G_k^l x_k^l \tag{4.57}$$

where $\mathbf{F}_k^n = \mathbf{I}_{2\times2}$, $\mathbf{F}_k^{nl} = \mathbf{0}_{2\times1}$, $\mathbf{F}_k^{ln} = \mathbf{0}_{1\times2}$ and $\mathbf{F}_k^l = 1$. In measurement model in (4.57), $\mathbf{g}_k^n(\cdot)$, and G_k^l correspond to $-h_k^{DB}\left(\mathbf{x}_k^n\right)$ and 1.

4.4 Numerical Simulation

4.4.1 Simulation Condition

In this section, to verify the advantages of the proposed TSPMF, numerical simulation is performed for terrain as shown in Fig. 4.3. The flight path is straight from the south to the north like a bold line and the flight velocity is 240m/s. The vertical attitude of vehicle is assumed to leveling. The resolution of the terrain map is 3 arcsec and it is assumed that there is not map error. The IMU is assumed navigation grade and the radar altimeter error is a white noise as shown in Table.4.2. The initial error and covariance of state variables are set equal the initial position errors which are set by 50m for latitude and longitude and 10m for height. The simulations are performed for 3D PMF, RBPMF, TSPMF and adaptive TSPMF (ATSPMF) which is combined grid support adaptation and TSPMF. The RBPMF and the 3D PMF are set to the nonlinear state variable for latitude and longitude, and the linear state variable for altitude. 30 times Monte-Carlo simulations are performed in Matlab and the computation time is its run time calculated by tic-toc function.

Table 4.2 IMU and Sensor Specifications

Sensor	Error component	Specification (1-σ)
Accelerometer	Bias	100μg
	Velocity random walk	12μg/rt(Hz)
Gyroscope	Bias	0.01deg/h
	Angular random walk	0.005deg/rt(h)
RADAR	White noise	10m

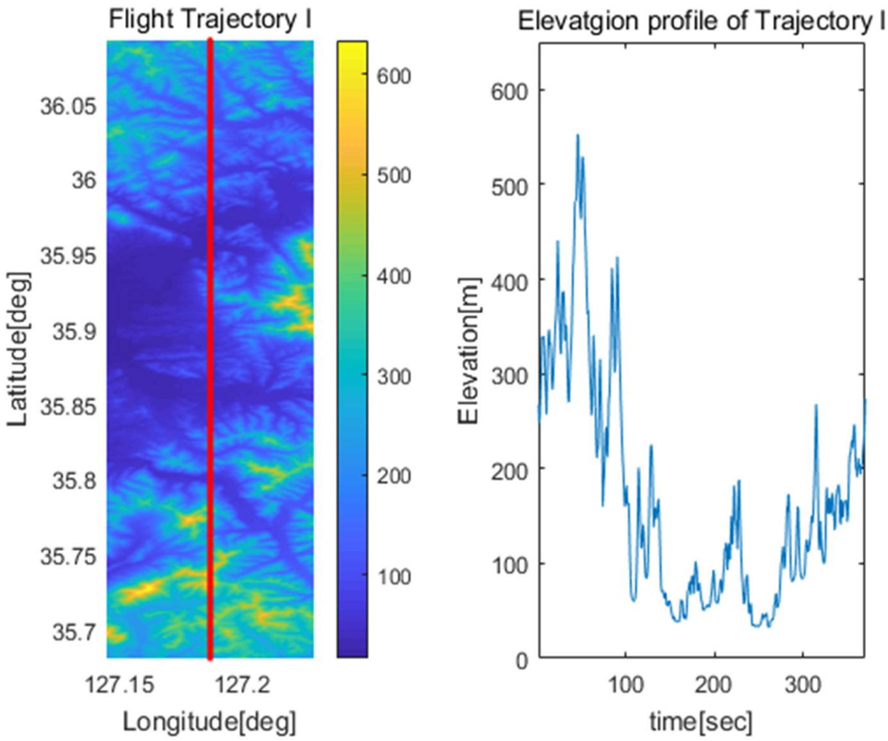

Figure 4.3 Terrain elevation map and elevation profile

4.4.2 Performance Comparison

As shown in Fig.4.4 and Fig.4.5, the results of each algorithm show almost similar performance in horizontal and vertical errors. In Table.4.3, horizontal error and vertical error does not differ greatly, but it shows differences in computation time. The results of the RBPMF show that the computation time is smaller than 3D PMF. This results in repetitive operations in time propagation for linear state variables, which consumes much computation time, because it is impossible to design the same kernel as in 2D PMF. In the case of general PMF, the computational time will increase exponentially when the state variable is augmented beyond 3D, but RBPMF will maintain above computation time. From the TSPMF results, the estimated performance is similar to that of 3D PMF, which is the most optimal result, and the computation time is drastically reduced because only one linear filter is used without any additional iteration. Like the RBPMF, even if more state variables are augmented, the computation time will be almost maintained, but the absolute computation time of TSPMF is overwhelmingly small. The ATSPMF results shows the most estimation performance and computation efficiency. The ATSPMF can be confirmed to be improved in estimation performance and calculation efficiency than TSPMF.

Table 4.3 Position error and computation time

Results	3D PMF	RBPMF	TSPMF	ATSPMF
Horizontal error [m]	16.61	16.93	16.80	16.33
Vertical error [m]	3.2	2.91	3.13	3.2

Computational time [sec]	56.63	54.87	47.72	45.86

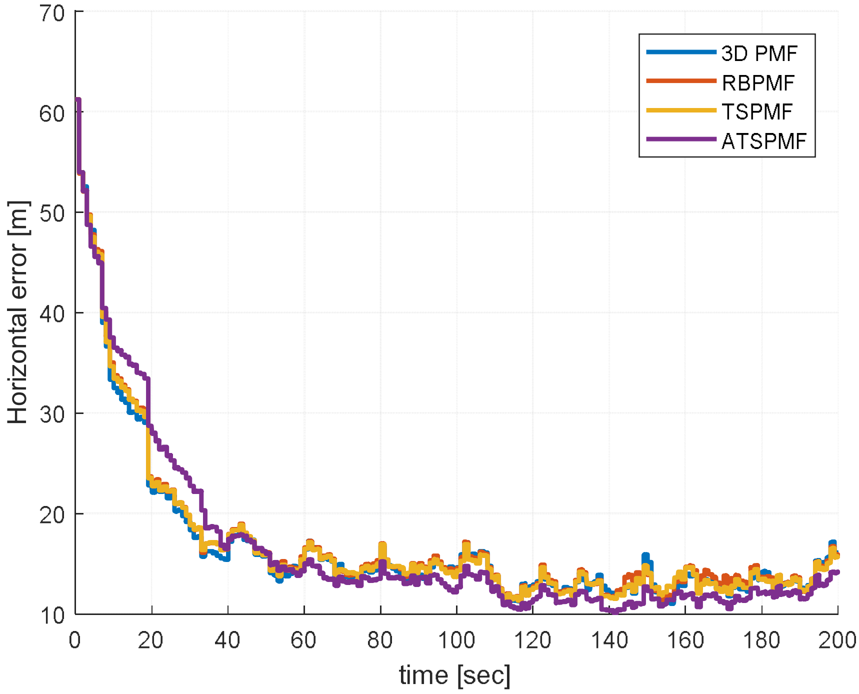

Figure 4.4   RMS horizontal position error

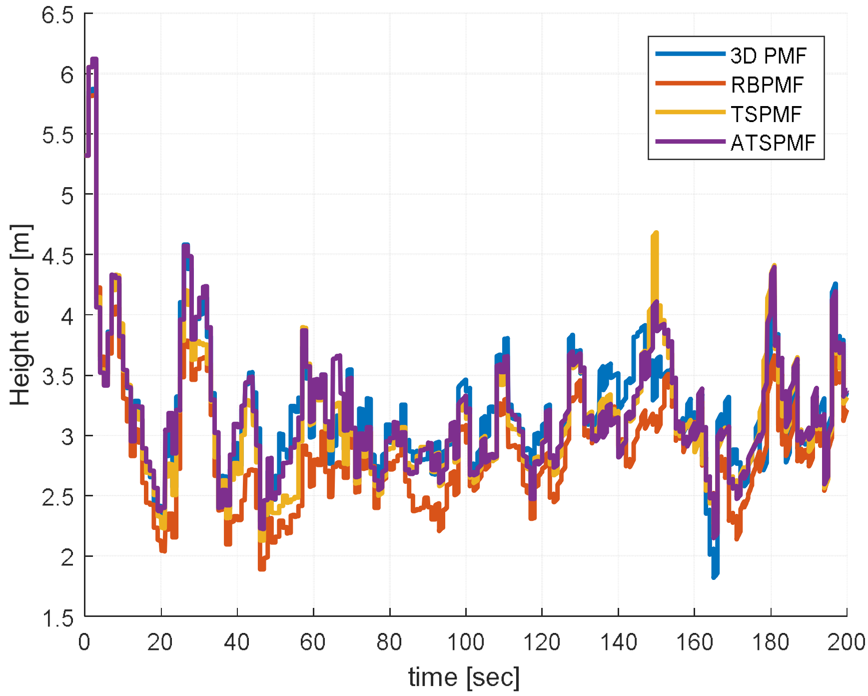

Figure 4.5 RMS vertical position error

4.4.2.1 Effect of Nonlinearity for Measurement Model

In order to estimate the linear stage variable h_k in the second stage of TSPMF, the Kalman gain $\mathbf{K}_k^n$ and the measurement matrix $\mathbf{H}_{d,k}$ for the nonlinear state variables of the first stage estimated using the PMF should be received. At this time, it cannot be calculated analytically, so we can get $\mathbf{K}_k^n$ and $\mathbf{H}_{d,k}$ by numerically as in sub-session 4.3.2. $\mathbf{H}_{d,k}$ is obtained through numerical differentiation, but if the nonlinearity of the measurement model is very severe, the filter might be unstable because the linearization error increase. To confirm the effect, simulations are performed by adding the unknown error of the white noise characteristic to the DEM. This error causes the true slope of the terrain to differ from the slope of the terrain using the DEM with error, so it can be seen that the linearization error is applied. DEM errors are set to 0, 10, 30, 50m white noise.

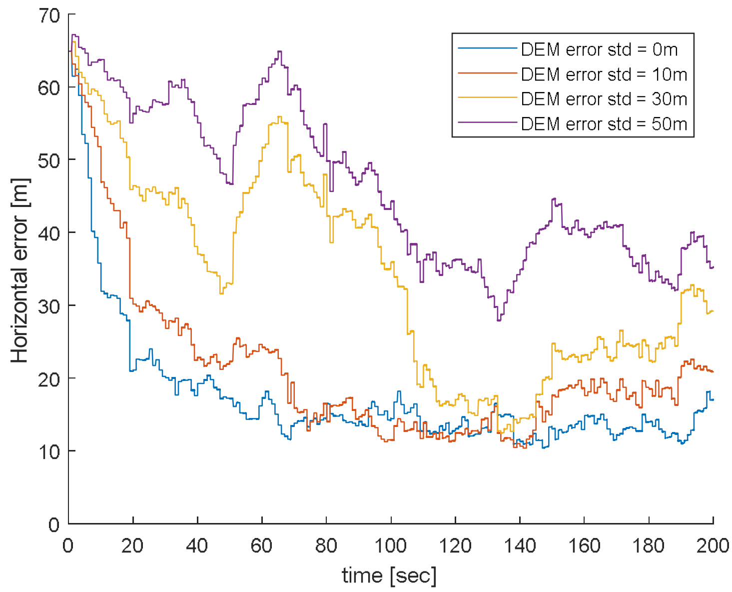

Figure 4.6 RMS horizontal position error with TSPMF

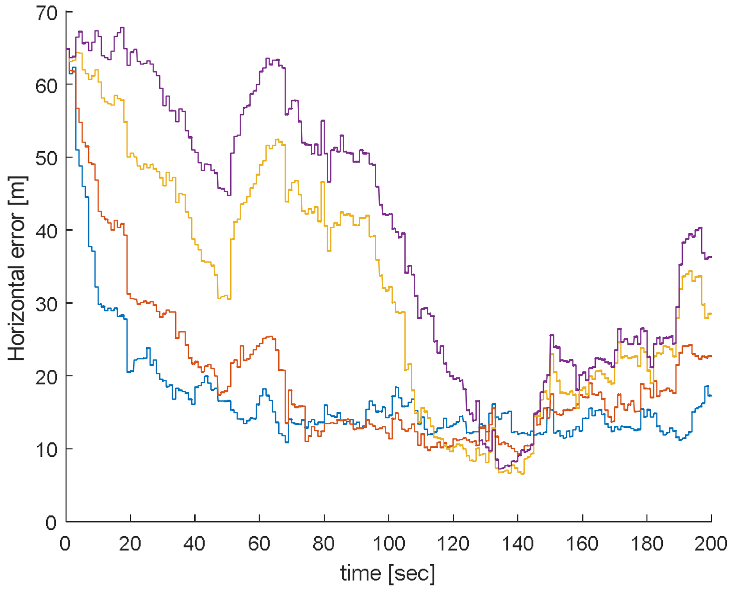

Figure 4.7   RMS horizontal position error with full-state PMF

As can be seen in figures 4.6 and 4.7, the results of TSPMF and full-state PMF are almost the same when the DEM error is small. However, as the DEM error increases, the error of the TSPMF increases. This is due to the linearization error. Since the level of DEM in recent years is less than 1 m in error with a resolution of about 10 m, it can be said that the influence of linearization error can be ignored.

4.4.2.2 Effect of Non-Gaussian Distribution of Prior PDF

Since the Kalman gain cannot be computed analytically in the PMF of the first stage, it is calculated through the moment matching as in Equation (4.45) - (4.49).

At this time, if the prior pdf $p\left(\mathbf{x}_k^{n,j} \mid \mathbf{Z}_{k-1}\right)$ deviates significantly from the Gaussian distribution, the Kalman gain estimation by the moment matching will be less accurate. Therefore, I adopt an index called Hellinger distance (HD) to analyze the similarity between the Gaussian distribution calculated through moment matching and the actual prior pdf. HD is calculated as an index to calculate the similarity of two probability distributions for two random variables $P = \{p_1, ..., p_n\}$ and $Q = \{q_1, ..., q_n\}$ as follows.

$$H(P,Q) = \frac{1}{\sqrt{2}} \sqrt{\sum_{j=1}^{N} \left(\sqrt{p_j} - \sqrt{q_j}\right)^2} \tag{4.58}$$

This value becomes closer to 0 as the probability distributions of the two are the same, and closer to 1 as they are different from each other. Using this index, I calculate the similarity of pdf obtained by using covariance calculated from moment matching and original prior pdf.

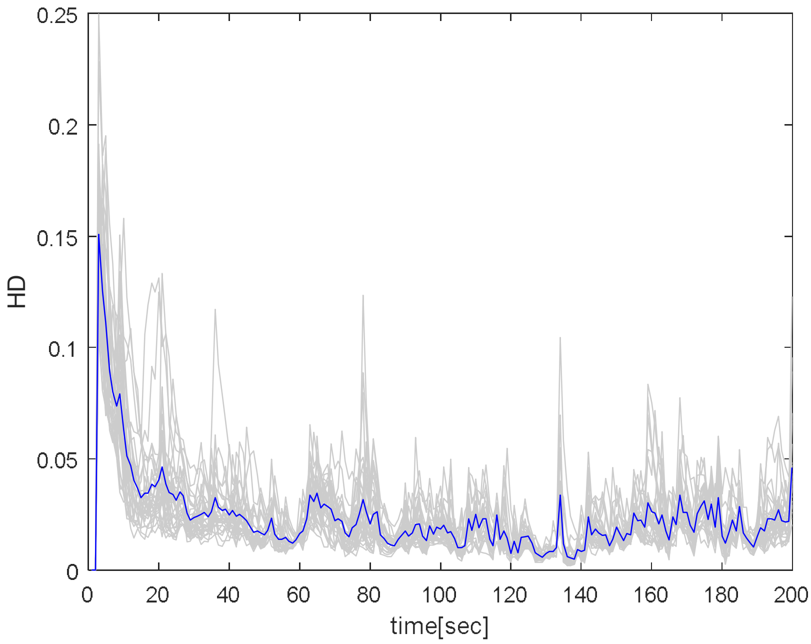

Figure 4.8 HD between original prior pdf and estimated prior pdf by moment matching

Figure 4.8 shows the HD in the trajectory I. It can be seen from this result that the HD value decreases below a very small value of less than 0.1 in the initial few seconds, and then it keeps a small value after the convergence of the filter thereafter. Therefore, although some performance degradation may occur initially in the TSPMF, the distribution of the PDF is generally Gaussian, so that there is few influence by non-Gaussian distribution of prior pdf.

4.5 Summary

TSPMF for state augmentation on TRN was proposed. PMF was suitable for application to TRN because it had robustness to large position error and nonlinearity of measurement equation. But it had a disadvantage of computation complexity when the state variables were augmented, so usually PMF used 2 or 3 state variables which were latitude and longitude or including height. The TSPMF is designed to maintain the estimated performance without imposing a computational burden even if the state variable is augmented. The nonlinear state variables, latitude and longitude, were estimated using the general PMF and linear state, altitude, was estimated using a single Kalman filter. At this time, specific information which are Kalman gain and prior covariance of nonlinear filter should be transferred to the linear filter, and converted into a form that can be used by using the moment matching. Simulation results showed that the estimation performance of 3D PMF, RB-PMF, and TSPMF was almost similar, but the computation time of TSPMF was overwhelmingly than RB-PMF. In this paper, we considered only three state variables because it was difficult to implement three or more dimensional PMF. However, if we apply the proposed algorithm, we can apply it to more than three dimensional state variables without degradation of estimation performance and computation burden.

Chapter 5

Conclusion

This dissertation has proposed the methods to improve the estimation performance and computation efficiency in PMF based TRN. For this purpose, grid support adaptation has proposed by considering measurement quality for performance improvement and computation efficiency. In addition, the TSPMF, which combine PMF and two stage filter, has proposed for state augmentation without heavy computation load.

In generally speaking, the estimation performance is improved when a large grid support size is applied because the probability density can be precisely expressed with large grid support. But, large grid support causes computational load heavy. It is because that the computational load is proportional to the square of the total number of grid points. But, in this dissertation, I have insisted that to adapt the size of the grid support considering measurement quality has been better. If the measurement quality is good in previous epoch, it advantageous to reduce the size of the grid support for computational efficiency. Contrary, if the measurement quality is bad in previous epoch, it is advantageous to increase the size of the grid support for estimation performance. At this time, the MI (mutual information), which is an index that determines the correlation between two random variables, is used for discrimination parameter for grid support adaptation. Therefore, the MI has been calculated for prior and posterior pdf, and judged that the measurement quality has been good when the value has been greater than 0. Conversely, when the value has been smaller than 0, it has been judged for bad the measurement quality. So, the adaptation algorithm is that if the MI is larger than 0, then the size of the grid support increases, or if the MI is smaller than 0, then the size of the grid support decreases. By the grid support adaptation algorithm, the estimation performance has been improved and computation time has decreased.

Typically, almost previous PMF based TRN studies have used only latitude and longitude as two dimensional state variables. It is because that specific kernel is able to design for computation efficiency. Using this kernel, the time propagation can be done with a single matrix multiplication without iterations. But, in three or more dimensional state variables, the specific kernel cannot be designed, so a lot of iterations is needed. To solve this problem, the TSPMF (two stage point mass filter) has been proposed in this dissertation. The TSPMF has combined PMF and two stage filter. In first stage, the nonlinear state variables have been estimated by the general PMF. Next, in second stage, the linear state variables have been estimated by a single Kalman filter. At this time, error covariances and Kalman gain in first stage have been needed for the Kalman filter in second stage. But, since the PMF does not have matrix-type covariances and Kalman gain, it has been calculated through moment matching. TSPMF has been applied to TRN by setting latitude and longitude as nonlinear state variables and height as linear state variables. Simulations have been performed to compare the performance of full state 3 dimensional PMF, RBPMF, and TSPMF. As a result, the estimation performance was almost similar, showing a reduction. In addition, by applying grid support adaptation to TSPMF, additional performance improvement and computational efficiency have been shown.

Bibliography

[1] S. Garg, L. Morrow, and R. Mamen, "Strapdown Navigation Technology: A literature survey," *Journal of Guidance, Control, and Dynamics,* vol. 1, no. 3, pp. 161-172, 1978.

[2] A. King, "Inertial Navigation : Forty Years of Evolution," *GEC review,* vol. 13, no. 3, pp. 140-149, 1998.

[3] D. Titterton and J. L. Weston, *Strapdown Inertial Navigation Technology*, 2nd ed. IET, 2004.

[4] J. Wendel, O. Meister, C. Schlaile, and G. F. Trommer, "An Integrated GPS/MEMS-IMU Navigation System for an Autonomous Helicopter," *Aerospace Science and Technology,* vol. 10, no. 6, pp. 527-533, 2006.

[5] S. Gao, Y. Zhong, X. Zhang, and B. Shirinzadeh, "Multi-Sensor Optimal Data Fusion for INS/GPS/SAR Integrated Navigation System," *Aerospace Science and Technology,* vol. 13, no. 4-5, pp. 232-237, 2009.

[6] W. Wang, Z.-y. Liu, and R.-r. Xie, "Quadratic Extended Kalman Filter Approach for GPS/INS Integration," *Aerospace Science and Technology,* vol. 10, no. 8, pp. 709-713, 2006.

[7] Y. M. Yoo, J. G. Park, and C. G. Park, "A Theoretical Approach to Observability Analysis of the SDINS/GPS in Maneuvering with Horizontal Constant Velocity," *International Journal of Control, Automation and*

Systems, vol. 10, no. 2, pp. 298-307, 2012.

[8] A. Grant, P. Williams, N. Ward, and S. Basker, "GPS Jamming and the Impact on Maritime Navigation," *The Journal of Navigation,* vol. 62, no. 2, pp. 173-187, 2009.

[9] N. O. Tippenhauer, C. Pöpper, K. B. Rasmussen, and S. Capkun, "On the Requirements for Successful GPS Spoofing Attacks," in *Proceedings of the 18th ACM conference on Computer and communications security*, 2011, pp. 75-86: ACM.

[10] H. Hu and N. Wei, "A Study of GPS Jamming and Anti-jamming," in *Power Electronics and Intelligent Transportation System (PEITS), 2009 2nd International Conference on*, 2009, vol. 1, pp. 388-391: IEEE.

[11] A. J. Kerns, D. P. Shepard, J. A. Bhatti, and T. E. Humphreys, "Unmanned Aircraft Capture and Control via GPS Spoofing," *Journal of Field Robotics,* vol. 31, no. 4, pp. 617-636, 2014.

[12] I. Lowrey and J. Shellenbarger, "Passive Navigation Using Inertial Navigation Sensors and Maps," *Naval Engineers Journal,* vol. 109, no. 3, pp. 245-249, 1997.

[13] H. Rice, S. Kelmenson, and L. Mendelsohn, "Geophysical Navigation Technologies and Applications," in *Position Location and Navigation Symposium, 2004. PLANS 2004*, 2004, pp. 618-624: IEEE.

[14] Z. Wang and S. Bian, "A Local Geopotential Model for Implementation of Underwater Passive Navigation," *Progress in Natural Science,* vol. 18, no. 9, pp. 1139-1145, 2008.

[15] Y. Han, B. Wang, Z. Deng, and M. Fu, "An Improved TERCOM-Based

Algorithm for Gravity-Aided Navigation," *IEEE Sensors Journal,* vol. 16, pp. 2537-2544, 2016.

[16] B. Wang, L. Yu, Z. Deng, and M. Fu, "A Particle Filter-based Matching Algorithm with Gravity Sample Vector for Underwater Gravity Aided Navigation," *IEEE/ASME Transactions on Mechatronics,* vol. 21, no. 3, pp. 1399-1408, 2016.

[17] B. Wang, Y. Zhu, Z. Deng, and M. Fu, "The Gravity Matching Area Selection Criteria for Underwater Gravity-Aided Navigation Application Based on the Comprehensive Characteristic Parameter," *IEEE/ASME Transactions on Mechatronics,* vol. 21, no. 6, pp. 2935-2943, 2016.

[18] Y. Han, B. Wang, Z. Deng, S. Wang, and M. Fu, "A Mismatch Diagnostic Method for TERCOM-based Underwater Gravity Aided Navigation," *IEEE Sensors Journal,* vol. 17, no. 9, pp. 2880-2888, 2017.

[19] C. Tyren, "Magnetic Terrain Navigation," in *Unmanned Untethered Submersible Technology, Proceedings of the 1987 5th International Symposium on*, 1987, vol. 5, pp. 245-256: IEEE.

[20] J. B. Phillips, "Magnetic Navigation," *Journal of Theoretical Biology,* vol. 180, no. 4, pp. 309-319, 1996.

[21] M. m. Li, H. q. Lu, H. Yin, and X. l. Huang, "Novel Algorithm for Geomagnetic Navigation," *Journal of Central South University of Technology,* vol. 18, no. 3, pp. 791-799, 2011.

[22] A. Canciani and J. Raquet, "Absolute Positioning Using the Earth's Magnetic Anomaly Field," *Navigation,* vol. 63, no. 2, pp. 111-126, 2016.

[23] F. C. Teixeira, J. Quintas, and A. Pascoal, "Experimental Validation of

Magnetic Navigation of Marine Robotic Vehicles," *IFAC-PapersOnLine,* vol. 49, no. 23, pp. 273-278, 2016.

[24] A. Canciani and J. Raquet, "Airborne Magnetic Anomaly Navigation," *IEEE Transactions on Aerospace and Electronic Systems,* vol. 53, no. 1, pp. 67-80, 2017.

[25] J. Campbell, M. U. de Haag, and F. van Graas, "Terrain Referenced Precision Approach Guidance," in *Proceedings of the 2005 National Technical Meeting of The Institute of Navigation*, 2001, pp. 643-653.

[26] G. M. Siouris, *Missile Guidance and Control Systems*. Springer Science & Business Media, 2004.

[27] J. Campbell, M. U. Haag, and F. Graas, "Terrain-Referenced Precision Approach Guidance: Proof-of-Concept Flight Test Results," *Navigation,* vol. 54, no. 1, pp. 21-29, 2007.

[28] F. W. Riedel *et al.*, "Guidance and Navigation in the Global Engagement Department," *Johns Hopkins APL technical digest,* vol. 29, no. 2, pp. 118-132, 2010.

[29] D. Vaman, "TRN history, Trends and the Unused Potential," in *Digital Avionics Systems Conference (DASC), 2012 IEEE/AIAA 31st*, 2012, pp. 1A3-1-1A3-16: IEEE.

[30] M. W. Cannon Jr and J. W. Carl, "TERCOM Performance: Analysis and Simulation," AIR FORCE AEROSPACE MEDICAL RESEARCH LAB WRIGHT-PATTERSON AFB OH1974.

[31] N. Priestley, "Terrain Referenced Navigation," in *Position Location and Navigation Symposium, 1990. Record. The 1990's-A Decade of Excellence*

in the Navigation Sciences. IEEE PLANS'90., IEEE, 1990, pp. 482-489: IEEE.

[32] H. Rice, L. Mendelsohn, R. Aarons, and D. Mazzola, "Next Generation Marine Precision Navigation System," in *Position Location and Navigation Symposium, IEEE 2000*, 2000, pp. 200-206: IEEE.

[33] J. Metzger, O. Meister, G. F. Trommer, F. Tumbrägel, and B. Taddiken, "Adaptations of a Comparison Technique for Terrain Navigation," *Aerospace science and technology,* vol. 9, no. 6, pp. 553-560, 2005.

[34] V. Ekütekin, "Navigation and Control Studies on Cruise Missiles," phD thesis, Mechanical engineering, Middle East Technical University, 2007.

[35] S. H. Yun and C. G. Park, "Position Fix in Terrain Referenced Navigation Using Statistical Verification," *IET Radar, Sonar & Navigation,* vol. 8, no. 9, pp. 1091-1099, 2014.

[36] K. Zhang, Y. Li, J. Zhao, and C. Rizos, "A Study of Underwater Terrain Navigation Based on the Robust Matching Method," *The Journal of Navigation,* vol. 67, no. 4, pp. 569-578, 2014.

[37] L. Zhao, N. Gao, B. Huang, Q. Wang, and J. Zhou, "A Novel Terrain-Aided Navigation Algorithm Combined with the TERCOM Algorithm and Particle Filter," *IEEE Sensors Journal,* vol. 15, no. 2, pp. 1124-1131, 2015.

[38] L. Zhou, X. Cheng, and Y. Zhu, "Terrain Aided Navigation for Autonomous Underwater Vehicles with Coarse Maps," *Measurement Science and Technology,* vol. 27, no. 9, p. 095002, 2016.

[39] L. Hostetler and R. Beckmann, "Sandia Inertial Terrain-Aided Navigation System," 1977.

[40] L. Hostetler and R. Andreas, "Nonlinear Kalman Filtering Techniques for Terrain-Aided Navigation," *IEEE Transactions on Automatic Control,* vol. 28, no. 3, pp. 315-323, 1983.

[41] J. Hollowell, "Heli/SITAN: A Terrain Referenced Navigation Algorithm for Helicopters," in *Position Location and Navigation Symposium, 1990. Record. The 1990's-A Decade of Excellence in the Navigation Sciences. IEEE PLANS'90., IEEE*, 1990, pp. 616-625: IEEE.

[42] D. Simon, *Optimal State Estimation: Kalman, H infinity, and nonlinear approaches*. John Wiley & Sons, 2006.

[43] S. H. Mok and H. Bang, "Terrain Slope Estimation Methods Using the Least Squares Approach for Terrain Referenced Navigation," *International Journal Aeronautical and Space Sciences,* vol. 14, no. 1, pp. 85-90, 2013.

[44] S. Juler, J. Uhlmann, and H. Durrant-Whyte, "A New Method for Nonlinear Transformation of Means and Covariances in Filters and Estimator," *IEEE Trans. Autom. Control,* vol. 45, no. 3, pp. 477-482, 2000.

[45] J. Metzger, K. Wisotzky, J. Wendel, and G. Trommer, "Sigma-Point Filter for Terrain Referenced Navigation," in *AIAA Guidance, Navigation, and Control Conference and Exhibit*, 2005, p. 6068.

[46] F. Wei, Z. Yuan, and R. Zhe, "UKF-Based Underwater Terrain Matching Algorithms Combination," presented at the International Industrial Informatics and Computer Engineering Conference (IIICEC 2015) 2015.

[47] P.-J. Nordlund and F. Gustafsson, "Sequential Monte Carlo Filtering Techniques Applied to Integrated Navigation Systems," in *American Control Conference, 2001. Proceedings of the 2001*, 2001, vol. 6, pp. 4375-

4380: IEEE.

[48] F. Gustafsson *et al.*, "Particle Filters for Positioning, Navigation, and Tracking," *IEEE Transactions on signal processing,* vol. 50, no. 2, pp. 425-437, 2002.

[49] P.-J. Nordlund and F. Gustafsson, "Marginalized Particle Filter for Accurate and Reliable Terrain-Aided Navigation," *IEEE Transactions on Aerospace and Electronic Systems,* vol. 45, no. 4, 2009.

[50] F. Gustafsson, "Particle Filter Theory and Practice with Positioning Applications," *IEEE Aerospace and Electronic Systems Magazine,* vol. 25, no. 7, pp. 53-82, 2010.

[51] A. Murangira, C. Musso, and K. Dahia, "A Mixture Regularized Rao-Blackwellized Particle Filter for Terrain Positioning," *IEEE Transactions on Aerospace and Electronic Systems,* vol. 52, no. 4, pp. 1967-1985, 2016.

[52] B. Turan and A. T. Kutay, "Particle Filter Studies on Terrain Referenced Navigation," in *Position, Location and Navigation Symposium (PLANS), 2016 IEEE/ION*, 2016, pp. 949-954: IEEE.

[53] F. C. Teixeira, J. Quintas, P. Maurya, and A. Pascoal, "Robust Particle Filter Formulations with Application to Terrain-Aided Navigation," *International Journal of Adaptive Control and Signal Processing,* vol. 31, no. 4, pp. 608-651, 2017.

[54] S. C. Kramer and H. W. Sorenson, "Recursive Bayesian Estimation Using Piece-Wise Constant Approximations," *Automatica,* vol. 24, no. 6, pp. 789-801, 1988.

[55] N. Bergman, "Recursive Bayesian Estimation: Navigation and Tracking

Application," phD thesis, Department of Electrical Engineering, Linköping University, Linköping Studies in Science and Technology, 1999.

[56] N. Bergman, L. Ljung, and F. Gustafsson, "Terrain Navigation Using Bayesian Statistics," *IEEE control systems,* vol. 19, no. 3, pp. 33-40, 1999.

[57] N. Bergman and P. Tichavský, "Two Cramér-Rao Bounds for Terrain-Aided Navigation," *IEEE Transactions on Aerospace and Electronic Systems,* 1999.

[58] M. Simandl, J. Královec, and T. Soderstrom, "Anticipative Grid Design in Point-Mass Approach to Nonlinear State Estimation," *IEEE Transactions on Automatic Control,* vol. 47, no. 4, pp. 699-702, 2002.

[59] J. Královec and M. Šimandl, "Filtering, Prediction and Smoothing with Point-Mass Approach," *IFAC Proceedings Volumes,* vol. 37, no. 6, pp. 375-380, 2004.

[60] J. Královec and M. Ŝimandl, "Numerical Solution of Filtering Problem with Multimodal Densities," *IFAC Proceedings Volumes,* vol. 38, no. 1, pp. 242-247, 2005.

[61] M. Šimandl, J. Královec, and T. Söderström, "Advanced Point-Mass Method for Nonlinear State Estimation," *Automatica,* vol. 42, no. 7, pp. 1133-1145, 2006.

[62] B. Copp and K. Subbarao, "Nonlinear Adaptive Filtering in Terrain-Referenced Navigation," *IEEE Transactions on Aerospace and Electronic Systems,* vol. 51, no. 4, pp. 3461-3469, 2015.

[63] B. L. Copp, "Bayesian Statistics and Information Fusion for GPS-Denied Navigation," phD, The University of Texas at Arlington, 2015.

[64] Y. M. Yoo and C. G. Park, "Improvement of Terrain Referenced Navigation Using a Point Mass Filter with Grid Adaptation," *International Journal of Control, Automation and Systems,* vol. 13, no. 5, pp. 1173-1181, 2015.

[65] J. Dunik, M. Simandl, and O. Straka, "Unscented Kalman Filter: Aspects and Adaptive Setting of Scaling Parameter," *IEEE Transactions on Automatic Control,* vol. 57, no. 9, pp. 2411-2416, 2012.

[66] H. M. Menegaz, J. Y. Ishihara, G. A. Borges, and A. N. Vargas, "A Systematization of the Unscented Kalman Filter Theory," *IEEE Transactions on automatic control,* vol. 60, no. 10, pp. 2583-2598, 2015.

[67] R. G. Brown and P. Y. Hwang, t. ed., Ed. *Introduction to Random Signals and Applied Kalman Filtering: with MATLAB Exercises and Solutions*. New York: John Wiley & Sons, 2012.

[68] B. Ristic, S. Arulampalam, and N. Gordon, "Beyond the Kalman Filter," *IEEE Aerospace and Electronic Systems Magazine,* vol. 19, no. 7, pp. 37-38, 2004.

[69] Z. Chen, "Bayesian Filtering: From Kalman Filters to Particle Filters, and Beyond," *Statistics,* vol. 182, no. 1, pp. 1-69, 2003.

[70] M. S. Arulampalam, S. Maskell, N. Gordon, and T. Clapp, "A Tutorial on Particle Filters for Online Nonlinear/Non-Gaussian Bayesian Tracking," *IEEE Transactions on signal processing,* vol. 50, no. 2, pp. 174-188, 2002.

[71] U. Orguner, P. Skoglar, D. Törnqvist, and F. Gustafsson, "Combined Point-Mass and Particle Filter for Target Tracking," in *Aerospace Conference, 2010 IEEE*, 2010, pp. 1-10: IEEE.

[72] V. Šmídl and M. Gašperin, "Rao-Blackwellized Point Mass Filter for

Reliable State Estimation," in *Information Fusion (FUSION), 2013 16th International Conference on*, 2013, pp. 312-318: IEEE.

[73] Freidland, B., “Treatment of Bias in Recursive Filtering,” IEEE Transactions on Automatic Control, Vol. AC-14, August, 1969.

[74] Alouani, A. T., Xia, P., Rice, T. R., and Blair, W. D., “On the Optimality of Two-Stage State Estimation In the Presence of Random Bias,” IEEE Transactions on Automatic Control, vol. 38, No. 8, August, 1993.

[75] Alounai, A. T., Rice, T. R. and Blair, W. D., “A Two-Stage Filter for State Estimation in the Presence of Dynamic Stochastic Bias,” Proceedings of the 1992 American Control Conference, June 1992, 1784-1788.

[76] Kim, K. H., Lee, J. G., and Park, C. G., “Adaptive two-stage Kalman filter in the presence of unknown random bias,” International Journal of Adaptive Control and Signal Processing, Vol. 20, pp. 305-319, 2006

[77] Kim, K. H., Lee, J. G., and C. G. Park, “Adaptive Two-Stage EKF for INS-GPS Loosely Coupled System with Unknown Fault Bias,” Journal of Global Positioning System, Vol. 5, No. 1-2, pp.62-69, 2006

[78] Kim, K. H., Lee, J. G., and Park, C. G., “Adaptive Two-Stage Extended Kalman Filter fir a Fault-Toleranct INS-GPS Loosely Coupled System,” IEEE Transactions on Aerospace and Electronic Systems, Vol. 45, No. 1, January, 2009.

[79] Derek W. Robinson, “Entropy and Uncertainty”, Entropy, Vol. 10, No. 4, pp. 493-506